Inorg. Chem. **2009**, *48*, 607−620

Exchange Interactions and Zero-Field Splittings in C_3-Symmetric $Mn^{III}_6Fe^{III}$: Using Molecular Recognition for the Construction of a Series of High Spin Complexes Based on the Triplesalen Ligand

Thorsten Glaser,*,† Maik Heidemeier,† Erich Krickemeyer,† Hartmut Bögge,† Anja Stammler,† Roland Fröhlich,§ Eckhard Bill,‡ and Jürgen Schnack*,||

Lehrstuhl für Anorganische Chemie I, Fakultät für Chemie, Universität Bielefeld, Universitätsstr. 25, D-33615 Bielefeld, Germany, Organisch-Chemisches Institut, Westfälische Wilhelms-Universität, Corrensstr. 40, D-48149 Münster, Germany, Max-Planck-Institut für Bioanorganische Chemie, Stiftsstr. 34-36, D-45470 Mülheim, Germany, and Fakultät für Physik, Universität Bielefeld, Universitätsstr. 25, D-33615 Bielefeld, Germany

Received September 1, 2008

The reaction of the tris(tetradentate) triplesalen ligand $H_6talen^{t\text{-}Bu_2}$, which provides three salen-like coordination environments bridged in a *meta*-phenylene arrangement by a phloroglucinol backbone, with Mn^{II} salts under aerobic conditions affords, in situ, the trinuclear Mn^{III} triplesalen complexes $[(talen^{t\text{-}Bu_2})\{Mn^{III}(solv)_n\}_3]^{3+}$. These can be used as molecular building blocks in the reaction with $[Fe(CN)_6]^{3-}$ as a hexaconnector to form the heptanuclear complex $[\{(talen^{t\text{-}Bu_2})\text{-}\{Mn^{III}(solv)_n\}_3\}_2\{Fe^{III}(CN)_6\}]^{3+}$ ($[Mn^{III}_6Fe^{III}]^{3+}$). The regular ligand folding observed in the trinuclear triplesalen complexes preorganizes the three metal ions for the reaction of three facially coordinated nitrogen atoms of a hexacyanometallate and provides a driving force for the formation of the heptanuclear complexes $[M^t_6M^c]^{n+}$ (M^t, terminal metal ion of the triplesalen building block; M^c, central metal ion of the hexacyanometallate) by molecular recognition, as has already been demonstrated for the single-molecule magnet $[Mn^{III}_6Cr^{III}]^{3+}$. $[\{(talen^{t\text{-}Bu_2})(Mn^{III}(MeOH))_3\}_2\{Fe^{III}(CN)_6\}][Fe^{III}(CN)_6]$ (**1**) was characterized by single-crystal X-ray diffraction, FTIR, ESI- and MALDI-TOF-MS, Mössbauer spectroscopy, and magnetic measurements. The molecular structure of $[Mn^{III}_6Fe^{III}]^{3+}$ is overall identical to that of $[Mn^{III}_6Cr^{III}]^{3+}$ but exhibits a different ligand folding of the Mn^{III} salen subunits with a helical distortion. The Mössbauer spectra demonstrate a stronger distortion from octahedral symmetry for the central $[Fe(CN)_6]^{3-}$ in comparison to the ionic $[Fe(CN)_6]^{3-}$. At low temperatures in zero magnetic fields, the Mössbauer spectra show magnetic splittings indicative of slow relaxation of the magnetization on the Mössbauer time scale. Variable-temperature−variable-field and μ_{eff} versus T magnetic data have been analyzed in detail by full-matrix diagonalization of the appropriate spin-Hamiltonian, consisting of isotropic exchange, zero-field splitting, and Zeeman interaction taking into account the relative orientation of the **D** tensors. Satisfactory reproduction of the experimental data has been obtained for parameters sets $J_{Mn-Mn} = -(0.85 \pm 0.15)$ cm^{-1}, $J_{Fe-Mn} = +(0.70 \pm 0.30)$ cm^{-1}, and $D_{Mn} = -(3.0 \pm 0.7)$ cm^{-1}. Comparing these values to those of $[Mn^{III}_6Cr^{III}]^{3+}$ provides insight into why $[Mn^{III}_6Fe^{III}]^{3+}$ is not a single-molecule magnet.

Introduction

The considerable interest in the synthesis of magnetic materials based on molecular entities started with the observation that $[Cp_2{*}Fe]^+[TCNE]^-$ exhibits a spontaneous long-range ferromagnetic ordering with a Curie temperature T_C of 4.8 K.[1−3] Another milestone in the field of molecule-based magnets was the observation that $[Mn_{12}O_{12}(O_2CCH_3)_{16}\text{-}(OH_2)_4]$, Mn_{12},[4] exhibits a hysteresis in the magnetization of pure molecular origin[5,6] and was the first member of a

* Author to whom correspondence should be addressed. E-mail: thorsten.glaser@uni-bielefeld.de (T.G.); juergen.schnack@uni-bielefeld.de (J.S.).
† Universität Bielefeld, Fakultät für Chemie.
‡ Max-Planck-Institut.
§ Westfälische Wilhelms-Universität, Münster.
|| Universität Bielefeld, Fakultät für Physik.

(1) Miller, J. S.; Calabrese, J. C.; Epstein, A. J.; Bigelow, R. W.; Zhang, J. H.; Reiff, W. M. *J. Chem. Soc., Chem. Comm.* **1986**, 1026–1028.
(2) Miller, J. S.; Calabrese, J. C.; Rommelmann, H.; Chittipeddi, S.; Epstein, A. J.; Zhang, J. H.; Reiff, W. M. *J. Am. Chem. Soc.* **1987**, *109*, 769–781.
(3) Miller, J. S. *Inorg. Chem.* **2000**, *39*, 4392–4408.
(4) Lis, T. *Acta Crystallogr.* **1980**, *36*, 2042–2046.

10.1021/ic8016529 CCC: $40.75
Published on Web 12/15/2008

new class of molecular materials called single-molecule magnets (SMMs).[7−10] SMMs possess an energy barrier for spin reversal which causes a slow relaxation of the magnetization at low temperatures. The energy barrier originates from a ground state with large total spin S_t and large magnetic anisotropy with an easy axis of magnetization (phenomenologically parametrized by a negative zero-field splitting parameter D). Thermally, the direction of the magnetization can only be reversed by a pathway over the top of the energy barrier due to the $\Delta M_S = \pm 1$ selection rule. SMMs attracted the interest of physicists due to the occurrence of quantum tunneling of the magnetization manifested by unusual steplike features in the hysteresis loops.[11−13] This quantum tunneling may be related in the kinetic relaxation picture provided above to a pathway through the magnetic anisotropy barrier. While this tunneling process is of high interest from a fundamental perspective, it results in a loss of the magnetization information; that is, it increases the observed relaxation rates for spin reversal and thus reduces the blocking temperatures T_B. The probability of this tunneling mechanism is related to the rhombic component of the magnetic anisotropy expressed phenomenologically by E_{St}, which is exactly zero for complexes of at least C_3 molecular symmetry.

In order to match all necessary requirements for SMMs, we have designed the C_3-symmetric triplesalen ligand **C** (Scheme 1a),[14,15] which combines the 1,3,5-trihydroxybenzene (phloroglucinol) bridging unit **A** for ferromagnetic couplings and thus high spin ground states with the coordination environment of a salen ligand **B** for a pronounced magnetic anisotropy.[16−18] The design of the triplesalen ligand has been based on the following rationales: In order to ensure high spin ground states,[19] we are exploring synthetic strategies to enforce ferromagnetic interactions by (a) the double exchange mechanism[20−22] in face-sharing octahedra,[23−25]

Scheme 1. (a) The C_3-Symmetric Hybrid−Ligand Triplesalen **C** Comprised of the Phloroglucinol Bridging Unit **A** for High Spin Ground States by Ferromagnetic Coupling and of a Salen-Like Coordination Environment **B** for Single-Site Magnetic Anisotropy by Strong Tetragonal Ligand Fields and (b) the Triplesalen Ligand $H_6talen^{t\text{-}Bu_2}$ Used in This Study

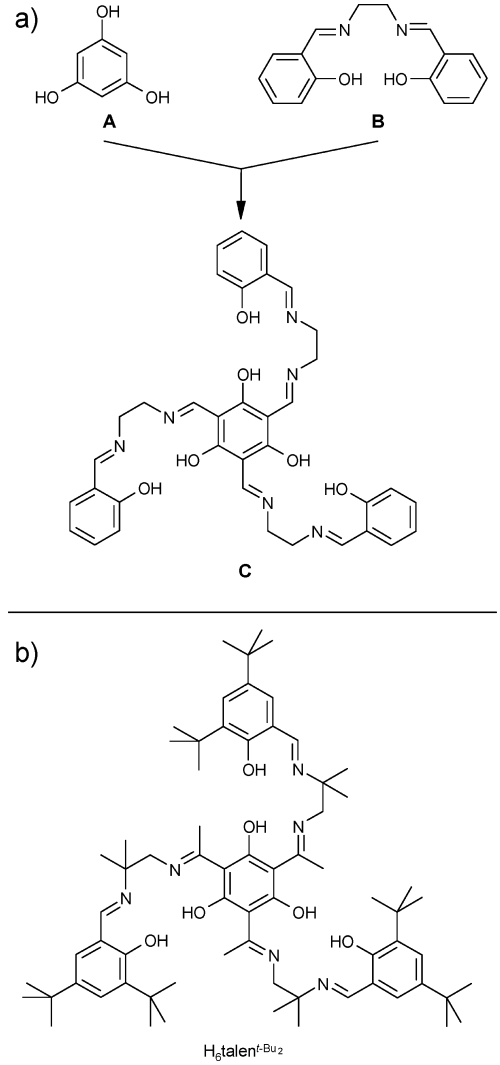

(b) the use of orthogonal magnetic orbitals,[26−28] and (c) the spin-polarization mechanism[29−34] in *m*-phenylene bridged

(5) Sessoli, R.; Gatteschi, D.; Caneschi, A.; Novak, M. A. *Nature* **1993**, *365*, 141–143.
(6) Sessoli, R.; Tsai, H. L.; Schake, A. R.; Wang, S. Y.; Vincent, J. B.; Folting, K.; Gatteschi, D.; Christou, G.; Hendrickson, D. N. *J. Am. Chem. Soc.* **1993**, *115*, 1804–1816.
(7) Christou, G.; Gatteschi, D.; Hendrickson, D. N.; Sessoli, R. *MRS Bull.* **2000**, *25*, 66–71.
(8) Long, J. R. In *Chemistry of Nanostructured Materials*; Yang, P., Ed.; World Scientific: Hong Kong, 2003; pp 291−315.
(9) Gatteschi, D.; Sessoli, R. *Angew. Chem., Int. Ed.* **2003**, *42*, 268–297.
(10) Gatteschi, D.; Sessoli, R.; Villain, J. *Molecular Nanomagnets*; Oxford University Press: Oxford, 2006.
(11) Thomas, L.; Lionti, F.; Ballou, R.; Gatteschi, D.; Sessoli, R.; Barbara, B. *Nature* **1996**, *383*, 145–147.
(12) Friedman, J. R.; Sarachik, M. P.; Tejada, J.; Maciejewski, J.; Ziolo, R. *J. Appl. Phys.* **1996**, *79*, 6031–6033.
(13) Friedman, J. R.; Sarachik, M. P.; Tejada, J.; Ziolo, R. *Phys. Rev. Lett.* **1996**, *76*, 3830–3833.
(14) Glaser, T.; Heidemeier, M.; Lügger, T. *Dalton Trans.* **2003**, 2381–2383.
(15) Glaser, T.; Heidemeier, M.; Fröhlich, R.; Hildebrandt, P.; Bothe, E.; Bill, E. *Inorg. Chem.* **2005**, *44*, 5467–5482.
(16) Kennedy, B. J.; Murray, K. S. *Inorg. Chem.* **1985**, *24*, 1552–1557.
(17) Mitra, S. *Prog. Inorg. Chem.* **1977**, *22*, 309–408.
(18) Bencini, A.; Ciofini, I.; Uytterhoeven, M. G. *Inorg. Chim. Acta* **1998**, *274*, 90–101.
(19) Kahn, O. *Acc. Chem. Res.* **2000**, *33*, 647–657.
(20) Zener, C. *Phys. Rev.* **1951**, *82*, 403–405.
(21) Blondin, G.; Girerd, J.-J. *Chem. Rev.* **1990**, *90*, 1359–1376.
(22) Glaser, T.; Rose, K.; Shadle, S. E.; Hedman, B.; Hodgson, K. E.; Solomon, E. I. *J. Am. Chem. Soc.* **2001**, *123*, 442–454.
(23) Beissel, T.; Birkelbach, F.; Bill, E.; Glaser, T.; Kesting, F.; Krebs, C.; Weyhermüller, T.; Wieghardt, K.; Butzlaff, C.; Trautwein, A. X. *J. Am. Chem. Soc.* **1996**, *118*, 12376–12390.
(24) Glaser, T.; Beissel, T.; Bill, E.; Weyhermüller, T.; Schünemann, V.; Meyer-Klaucke, W.; Trautwein, A. X.; Wieghardt, K. *J. Am. Chem. Soc.* **1999**, *121*, 2193–2208.
(25) Chibotaru, L. F.; Girerd, J.-J.; Blondin, G.; Glaser, T.; Wieghardt, K. *J. Am. Chem. Soc.* **2003**, *125*, 12615–12630.
(26) Kanamori, J. *J. Phys. Chem. Solids* **1959**, *10*, 87–98.
(27) Kahn, O. *Inorg. Chim. Acta* **1982**, *62*, 3–14.
(28) Glaser, T.; Theil, H.; Liratzis, I.; Weyhermüller, T.; Bill, E. *Inorg. Chem.* **2006**, *45*, 4889–4891.
(29) Longuet-Higgins, H. C. *J. Chem. Phys.* **1950**, *18*, 265–274.
(30) Iwamura, H. *Adv. Phys. Org. Chem.* **1990**, *26*, 179–253.
(31) Yoshizawa, K.; Hoffmann, R. *J. Am. Chem. Soc.* **1995**, *117*, 6921–6926.
(32) Iwamura, H.; Koga, N. *Acc. Chem. Res.* **1993**, *26*, 346–351.
(33) Dougherty, D. A. *Acc. Chem. Res.* **1991**, *24*, 88–94.
(34) Ovchinnikov, A. A. *Theor. Chim. Acta* **1978**, *47*, 297–304.

complexes.[35−38] We have shown that modified phloroglucinol ligands with pendant arms enable ferromagnetic interactions in trinuclear Cu^{II} complexes by the spin-polarization mechanism.[39] This principle of using *m*-phenylene bridging units to enforce ferromagnetic interactions by the spin-polarization mechanism has also been applied to transition metal complexes by other research groups.[40−58]

We have chosen a salen-like coordination environment because the salen ligand **B** is known to establish pronounced magnetic anisotropies by its strong ligand field in the basal plane.[16−18] A well studied example is the Jacobsen catalyst $[(salen')Mn^{III}Cl]$[59] (H_2salen' = (*R*,*R*)-N,N′-bis(3,5-di-*tert*-butylsalicylidene)-1,2-cyclohexanediamine), which is a Mn^{III} ($S = 2$) species with a zero-field splitting of $D \approx -2.5$ cm^{-1}.[16,60,61] In this respect, it is interesting to note that already dimeric Mn^{III} salen complexes behave as SMMs.[62]

The magnetic anisotropy of the ground state (D_{S_t}) of an exchange-coupled polynuclear complex attains its main component usually from the projection of the single site anisotropies (D_i) onto the spin ground state S_t, while dipolar and anisotropic interactions yield only minor contributions.[18,63] Since zero-field splittings are tensor quantities, the projection of the single-site zero-field splittings onto the spin ground state may vanish when the metal ion arrangement approaches a cubic symmetry.

In summary, a rational design of SMMs requires not only the realization of a high spin ground state S_t and a source of magnetic anisotropy but also a control of the molecular topology. In order to minimize the quantum mechanical magnetization tunneling, the complex should be at least C_3-symmetric, but the symmetry should be lower than cubic to prevent the absence of magnetic anisotropy of the coupled spin system. The increase of the number of metal ions in polynuclear metal complexes using small ligands with little influence on the directionality of the metal−ligand bond may lead to fascinating new complex structures by serendipity,[64] but these complexes tend to a highly symmetric arrangement of the metal ions.[65] By approaching a cubic point group symmetry, the local magnetic anisotropy tensors may cancel each other by projecting onto the total spin ground state.[63] The newly arising paradigm that the increase of the nuclearity of the complexes correlates with a decrease of the magnetic anisotropy and thus the blocking temperatures is therefore not an intrinsic property but a consequence where the central metal ligand core approaches a cubic arrangement if the ligand is not providing some steric requirements.

We have shown in a series of trinuclear triplesalen complexes of the ligand $H_6talen^{t\text{-}Bu_2}$ (Scheme 1b) that (*i*) the C_3-symmetry of the triplesalen ligand is impeded in the complex and (*ii*) a severe ligand folding occurs in $[(talen^{t\text{-}Bu_2})M_3]$ (M = Cu, Ni), resulting in an overall bowl-shaped molecular structure.[15,37] We have taken advantage of the ligand folding in the triplesalen complexes by reacting two trinuclear Mn^{III} triplesalen complexes $[(talen^{t\text{-}Bu_2})\{Mn^{III}(solv)_n\}_3]^{3+}$ as molecular building blocks with $[Cr(CN)_6]^{3-}$ as a hexaconnector.[66] Hexacyanometallates are well-known for their ability to bridge transition metal fragments like metal−salen units to 0D, 1D, 2D, or 3D structures with

(35) Glaser, T.; Gerenkamp, M.; Fröhlich, R. *Angew. Chem., Int. Ed.* **2002**, *41*, 3823–3825.
(36) Glaser, T.; Heidemeier, M.; Grimme, S.; Bill, E. *Inorg. Chem.* **2004**, *43*, 5192–5194.
(37) Glaser, T.; Heidemeier, M.; Strautmann, J. B. H.; Bögge, H.; Stammler, A.; Krickemeyer, E.; Huenerbein, R.; Grimme, S.; Bothe, E.; Bill, E. *Chem.—Eur. J.* **2007**, *13*, 9191–9206.
(38) Theil, H.; Frhr. v. Richthofen, C.-G.; Stammler, A.; Bögge, H.; Glaser, T. *Inorg. Chim. Acta* **2008**, *361*, 916–924.
(39) Glaser, T.; Theil, H.; Heidemeier, M. *C. R. Chimie* **2008**, *11*, 1121–1136.
(40) Francesconi, L. C.; Corbin, D. R.; Hendrickson, D. N.; Stucky, G. D. *Inorg. Chem.* **1979**, *18*, 3074–3080.
(41) Oshio, H. *J. Chem. Soc., Chem. Comm.* **1991**, 240–241.
(42) Oshio, H.; Ichida, H. *J. Phys. Chem.* **1995**, *99*, 3294–3302.
(43) McCleverty, J. A.; Ward, M. D. *Acc. Chem. Res.* **1998**, *31*, 842–851.
(44) Cargill Thompson, A. M. W.; Gatteschi, D.; McCleverty, J. A.; Navas, J. A.; Rentschler, E.; Ward, M. D. *Inorg. Chem.* **1996**, *35*, 2701–2703.
(45) Bayly, S. R.; Humphrey, E. R.; de Chair, H.; Paredes, C. G.; Bell, Z. R.; Jeffery, J. C.; McCleverty, J. A.; Ward, M. D.; Totti, F.; Gatteschi, D.; Courric, S.; Steele, B. R.; Screttas, C. G. *J. Chem. Soc., Dalton Trans.* **2001**, 1401–1414.
(46) Ung, V. A.; Thompson, A.; Bardwell, D. A.; Gatteschi, D.; Jeffery, J. C.; McCleverty, J. A.; Totti, F.; Ward, M. D. *Inorg. Chem.* **1997**, *36*, 3447–3454.
(47) Ung, V. A.; Couchman, S. M.; Jeffery, J. C.; McCleverty, J. A.; Ward, M. D.; Totti, F.; Gatteschi, D. *Inorg. Chem.* **1999**, *38*, 365–369.
(48) Fernández, I.; Ruiz, R.; Faus, J.; Julve, M.; Lloret, F.; Cano, J.; Ottenwaelder, X.; Journaux, Y.; Munoz, C. *Angew. Chem., Int. Ed.* **2001**, *40*, 3039–3042.
(49) Ottenwaelder, X.; Cano, J.; Journaux, Y.; Riviere, E.; Brennan, C.; Nierlich, M.; Ruiz-Garcia, R. *Angew. Chem., Int. Ed.* **2004**, *43*, 850–852.
(50) Pardo, E.; Morales-Osorio, I.; Julve, M.; Lloret, F.; Cano, J.; Ruiz-Garcia, R.; Pasan, J.; Ruiz-Perez, C.; Ottenwaelder, X.; Journaux, Y. *Inorg. Chem.* **2004**, *43*, 7594–7596.
(51) Pardo, E.; Bernot, K.; Julve, M.; Lloret, F.; Cano, J.; Ruiz-Garcia, R.; Pasán, J.; Ruiz-Perez, C.; Ottenwaelder, X.; Journaux, Y. *Chem. Comm.* **2004**, 920–921.
(52) Pereira, C. L. M.; Pedroso, E. F.; Stumpf, H. O.; Novak, M. A.; Ricard, L.; Ruiz-Garcia, R.; Rivière, E.; Journaux, Y. *Angew. Chem., Int. Ed.* **2004**, *43*, 956–958.
(53) Paital, A. R.; Mitra, T.; Ray, D.; Wong, W. T.; Ribas-Ariño, J.; Novoa, J. J.; Ribas, J.; Aromi, G. *Chem. Comm.* **2005**, 5172–5174.
(54) Mitsubori, S.-I.; Ishida, T.; Nogami, T.; Iwamura, H. *Chem. Lett.* **1994**, 285–288.
(55) Lloret, F.; De Munno, G.; Julve, M.; Cano, J.; Ruiz, R.; Caneschi, A. *Angew. Chem., Int. Ed.* **1998**, *37*, 135–138.
(56) Ishida, T.; Nakayama, K.; Nakagawa, M.; Sato, W.; Ishikawa, Y. *Synth. Met.* **1997**, *85*, 1655–1658.
(57) Ishida, T.; Mitsubori, S.-I.; Nogami, T.; Takeda, N.; Ishikawa, M.; Iwamura, H. *Inorg. Chem.* **2001**, *40*, 7059–7064.
(58) Foxon, S. P.; Torres, G. R.; Walter, O.; Pedersen, J. Z.; Toftlund, H.; Hüber, M.; Falk, K.; Haase, W.; Cano, J.; Lloret, F.; Julve, M.; Schindler, S. *Eur. J. Inorg. Chem.* **2004**, 335–343.
(59) Zhang, W.; Jacobsen, E. N. *J. Org. Chem.* **1991**, *56*, 2296–2298.
(60) Campbell, K. A.; Lashley, M. R.; Wyatt, J. K.; Nantz, M. H.; Britt, R. D. *J. Am. Chem. Soc.* **2001**, *123*, 5710–5719.
(61) Krzystek, J.; Telser, J. *J. Magn. Reson.* **2003**, *162*, 454–465.
(62) Miyasaka, H.; Clerac, R.; Wernsdorfer, W.; Lecren, L.; Bonhomme, C.; Sugiura, K.-I.; Yamashita, M. *Angew. Chem., Int. Ed.* **2004**, *43*, 2801–2805.
(63) Bencini, A.; Gatteschi, D. *Electron Paramagnetic Resonance of Exchanged Coupled Systems*; Springer-Verlag: Berlin, 1990.
(64) Winpenny, R. E. P. *J. Chem. Soc., Dalton Trans.* **2002**, 1–10.
(65) Powell, A. K. *Struct. Bonding (Berlin)* **1997**, *88*, 1–38.
(66) Glaser, T.; Heidemeier, M.; Weyhermüller, T.; Hoffmann, R.-D.; Rupp, H.; Müller, P. *Angew. Chem., Int. Ed.* **2006**, *45*, 6033–6037.
(67) Miyasaka, H.; Matsumoto, N.; Okawa, H.; Re, N.; Gallo, E.; Floriani, C. *J. Am. Chem. Soc.* **1996**, *118*, 981–994.
(68) Re, N.; Gallo, E.; Floriani, C.; Miyasaka, H.; Matsumoto, N. *Inorg. Chem.* **1996**, *35*, 6004–6008.
(69) Miyasaka, H.; Ieda, H.; Matsumoto, N.; Re, N.; Crescenzi, R.; Floriani, C. *Inorg. Chem.* **1998**, *37*, 255–263.
(70) Re, N.; Crescenzi, R.; Floriani, C.; Miyasaka, H.; Matsumoto, N. *Inorg. Chem.* **1998**, *37*, 2717–2722.
(71) Miyasaka, H.; Matsumoto, N.; Re, N.; Gallo, E.; Floriani, C. *Inorg. Chem.* **1997**, *36*, 670–676.

Scheme 2. Building Block Approach for the Construction of the Heptanuclear Complexes $[M^t_6M^c]^{n+a}$

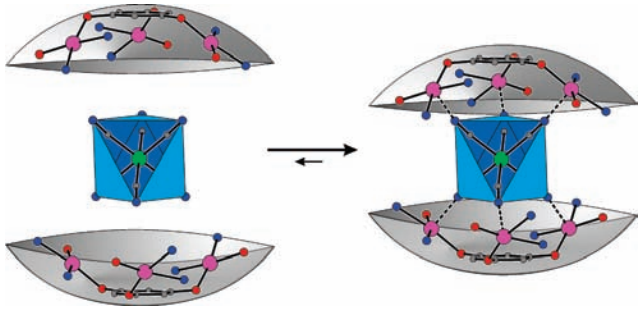

[a] The bowl-shaped structure of the trinuclear triplesalen building blocks preorganizes the three metal ions for coordination to the N atoms of a hexacyanometallate. This molecular recognition provides a driving force for the formation of the heptanuclear complex in analogy to the key−lock principle.

interesting magnetic properties.[8,67−77] Long et. al demonstrated that even a trinuclear complex constructed by two Mn^{III} salen complexes, which are bridged by a central $[Fe(CN)_6]^{3-}$, acts as a SMM due to the ferromagnetic $S_t = 9/2$ spin ground state, the local magnetic anisotropy of the Mn^{III} salen units, and the linear topology.[78] Miyasaka et al. used these trinuclear building blocks to form 1D chains, which exhibit single-chain magnetic behavior.[79,80]

Despite the success of the combination of metal salen units with hexacyanometallates and the highly predictable exchange coupling through a CN^- bridge,[72,81,82] the nuclearity and dimensionality of these complexes is difficult to control. In this respect, the advantage of our trinuclear building block $[(talen^{t\text{-}Bu_2})\{Mn^{III}(solv)_n\}_3]^{3+}$ is the ligand folding, which preorganizes the three Mn^{III} ions for the coordination of three facial nitrogen atoms of a hexacyanometallate $[M(CN)_6]^{n-}$ and should therefore result in a driving force for the formation of heptanuclear complexes $[M^t_6M^c]^{n+}$ (M^t, terminal metal ion of the triplesalen building block; M^c, central metal ion of the hexacyanometallate) by molecular recognition (Scheme 2).

The reaction of the 2 equiv of the molecular building block $[(talen^{t\text{-}Bu_2})\{Mn^{III}(solv)_n\}_3]^{3+}$ with 1 equiv of $[Cr(CN)_6]^{3-}$ resulted in the formation of the heptanuclear complex $[\{(talen^{t\text{-}Bu_2})Mn^{III}{}_3\}_2\{Cr^{III}(CN)_6\}]^{3+}$ ($[Mn^{III}{}_6Cr^{III}]^{3+}$), which was isolated as its BPh_4^- salt. AC susceptibility and hysteresis measurements proved $[Mn^{III}{}_6Cr^{III}]^{3+}$ to be a SMM with a high anisotropy barrier.[66] The simulation of the temperature dependence of the magnetic properties of $[Mn^{III}{}_6Cr^{III}]^{3+}$ showed that the coupling between the Mn^{III} ions in a trinuclear Mn^{III} triplesalen building block is slightly antiferromagnetic and not—as expected—ferromagnetic. Due to the large Hilbert space (62 500), only a spin-Hamiltonian consisting of an isotropic Heisenberg−Dirac−Van Vleck (HDvV) term and a Zeeman term has been used. Due to the neglect of zero-field splitting terms, only data above 50 K have been used to obtain the exchange coupling parameters. On the other hand, due to the small Hilbert space (125), we have been able to perform a thorough analysis for the nitro-substituted trinuclear Mn^{III} triplesalen complex $[(talen^{NO_2})\{Mn^{III}(DMSO)_2\}_3](ClO_4)_3$.[83] We have simulated temperature-dependent magnetic susceptibilities and variable-temperature−variable-field (VTVH) magnetization data using the appropriate spin-Hamiltonian including zero-field splitting by a full-matrix diagonalization approach. This provided also a weak antiferromagnetic interaction $J = -0.30 \pm 0.05$ cm^{-1} between the Mn^{III} ions but a strong magnetic anisotropy of each Mn^{III} ion expressed by $D = -4.0 \pm 0.4$ cm^{-1}.[83]

Here, we show that the formation of $[Mn^{III}{}_6Cr^{III}]^{3+}$ was not a singularity but that the molecular recognition by the preorganization of the three molecular building blocks in analogy to the key−lock principle provides a strong driving force for the generation of heptanuclear complexes of the general formula $[M^t_6M^c]^{n+}$. In this respect, the reaction of $[(talen^{t\text{-}Bu_2})\{Mn^{III}(solv)_n\}_3]^{3+}$ with $[Fe(CN)_6]^{3-}$ resulted in the formation of $[\{(talen^{t\text{-}Bu_2})Mn^{III}{}_3\}_2\{Fe^{III}(CN)_6\}]^{3+}$ ($[Mn^{III}{}_6Fe^{III}]^{3+}$) isolated as its $[Fe(CN)_6]^{3-}$ salt. In order to obtain reliable values for the exchange coupling constants J and the local magnetic anisotropies D, we have analyzed the magnetic data with the appropriate spin-Hamiltonian including HDvV, zero-field splitting, and Zeeman terms by full-matrix diagonalization. The relative orientations of the local D tensors have been incorporated by employing the local Jahn−Teller axes of the Mn^{III} ions.

Experimental Section

Preparation of Compounds. $H_6talen^{t\text{-}Bu_2}$ {= 2,4,6-tris{1-[2-(3,5-di-*tert*-butylsalicylaldimino)-2-methylpropylimino]-ethyl}−1,3,5-trihydroxybenzene} was synthesized as described previously.[14,15]

$[\{(talen^{t\text{-}Bu_2})(Mn^{III}(MeOH))_3\}_2\{Fe^{III}(CN)_6\}][Fe^{III}(CN)_6]$ (1). A solution of 147 mg (0.600 mmol) of $Mn(OAc)_2 \cdot 4H_2O$ in methanol (50 mL) was added to a stirred suspension of 222 mg (0.200 mmol) of $H_6talen^{t\text{-}Bu_2}$ in methanol (50 mL). Heating the mixture to reflux for 20 min resulted in a brown solution. After cooling to room temperature, the reaction solution was treated dropwise with a solution of 132 mg (0.401 mmol) of $K_3[Fe(CN)_6]$ and 1.00 g (3.78 mmol) of 18-crown-6 in methanol (50 mL).

After standing for 5 days, the precipitated crystals (polyeders with some hexagonal faces) and a powder were again heated to reflux in the mother liquor for a short time. The hot suspension

(72) Verdaguer, M.; Bleuzen, A.; Marvaud, V.; Vaissermann, J.; Seuleiman, M.; Desplanches, C.; Scuiller, A.; Train, C.; Garde, R.; Gelly, G.; Lomenech, C.; Rosenman, I.; Veillet, P.; Cartier, C.; Villain, F. *Coord. Chem. Rev.* **1999**, *190−192*, 1023–1047.
(73) Ohba, M.; Okawa, H. *Coord. Chem. Rev.* **2000**, *198*, 313–328.
(74) Beltran, L. M. C.; Long, J. R. *Acc. Chem. Res.* **2005**, *38*, 325–334.
(75) Rebilly, J.-N.; Mallah, T. *Struct. Bonding (Berlin)* **2006**, *122*, 103–131.
(76) Schelter, E. J.; Prosvirin, A. V.; Dunbar, K. R. *J. Am. Chem. Soc.* **2004**, *126*, 15004–15005.
(77) Palii, A. V.; Ostrovsky, S. M.; Klokishner, S. I.; Tsukerblat, B. S.; Berlinguette, C. P.; Dunbar, K. R.; Galán-Mascarós, J. R. *J. Am. Chem. Soc.* **2004**, *126*, 16860–16867.
(78) Choi, H. J.; Sokol, J. J.; Long, J. R. *Inorg. Chem.* **2004**, *43*, 1606–1608.
(79) Ferbinteanu, M.; Miyasaka, H.; Wernsdorfer, W.; Nakata, K.; Sugiura, K.-I.; Yamashita, M.; Coulon, C.; Clerac, R. *J. Am. Chem. Soc.* **2005**, *127*, 3090–3099.
(80) Coulon, C.; Miyasaka, H.; Clérac, R. *Struct. Bonding (Berlin)* **2006**, *122*, 163–206.
(81) Dunbar, K. R.; Heintz, R. A. *Prog. Inorg. Chem.* **1997**, *45*, 283–391.
(82) Weihe, H.; Güdel, H. U. *Comments Inorg. Chem.* **2000**, *1−2*, 75.
(83) Glaser, T.; Heidemeier, M.; Fröhlich, R. *C. R. Chim.* **2007**, *10*, 71–78.

Table 1. Crystallographic Data for $1\cdot 2H_2O\cdot 18MeOH$

empirical formula	$[C_{138}H_{192}N_{12}O_{12}Mn_6(CH_3OH)_6Fe(CN)_6]$-$[Fe(CN)_6]\cdot 2H_2O\cdot 18MeOH$
fw	3769.66
cryst syst	monoclinic
space group	$P2_1/c$
a (Å)	17.7464(7)
b (Å)	30.9994(11)
c (Å)	18.9839(7)
β (deg)	102.870(1)
V (Å^3)	10181.2(7)
Z	2
T (K)	183(2)
D_{calcd} (Mg/m^3)	1.230
μ(Mo Kα) (mm^{-1})	0.569
cryst size (mm)	0.42 × 0.40 × 0.32
θ range (deg)	1.57 to 26.99
reflns collected	60081
independent reflns	21992 (R(int) = 0.0341)
obs reflns ($I > 2\sigma(I)$)	16859
parameters	1126
goodness-of-fit on F^2	1.044
R1/wR2 ($I > 2\sigma(I)$)	0.0510/0.1395
max/min residuals (e × Å^{-3})	0.870/−0.533

was filtered, and the brown filtrate was standing at room temperature for 5 days with minimal evaporation of the solvent. Only crystals (polyhedra with some hexagonal faces) precipitated, which were separated. Single-crystals for X-ray diffraction studies were maintained in contact with the mother liquor to prevent solvent loss and were identified crystallographically as $1\cdot 2H_2O\cdot 18MeOH$. The other measurements were performed on a vaccuum-dried sample, which analyzed as $1\cdot 2H_2O\cdot 11MeOH$. Yield: 82 mg (23%). ESI-MS (MeOH): m/z (%) 917.5 (100) $[\{(talen^{t\text{-}Bu_2})Mn_3\}_2\{Fe(CN)_6\}]^{3+}$, 1376.2 (15) $[\{(talen^{t\text{-}Bu_2})Mn_3\}_2\{Fe(CN)_6\}]^{2+}$. MALDI-TOF-MS (matrix DCTB): m/z (%) 2751.0 (100) $[\{(talen^{t\text{-}Bu2})Mn_3\}_2\{Fe(CN)_6\}]^{+}$. IR (KBr): $\tilde{\nu}$ = 2953m, 2907m, 2868m, 2135m, 2106m, 2062m, 2027vw, 1614s, 1572s, 1537m, 1493vs, 1433m, 1393m, 1364m, 1339w, 13102m, 1275s, 1254s, 1188m, 1153m, 1060w, 1026w, 845m, 750w, 642w, 575m, 550m. Elem anal. (%) calcd for $1\cdot 2H_2O\cdot 11MeOH$ ($C_{167}H_{264}N_{24}O_{31}Fe_2Mn_6$): C, 56.58; H, 7.51; N, 9.48. Found: C, 56.60; H, 7.22; N, 9.13.

X-Ray Crystallography. Crystals of $1\cdot 2H_2O\cdot 18MeOH$ were mounted in a cold nitrogen stream (183(2) K) on a Bruker AXS SMART diffractometer (three-circle goniometer with 1 K CCD detector, Mo Kα radiation, graphite monochromator; hemisphere data collection in ω at 0.3° scan width in three runs with 606, 435, and 230 frames (ϕ = 0, 88, and 180°) at a detector distance of 5 cm). An empirical absorption correction using equivalent reflections was performed with the program SADABS 2.10.[84] The structure was solved with the program SHELXS-97[85,86] and refined on F^2 using SHELXL-97.[86] Hydrogen atoms were refined on calculated positions; no hydrogen atoms were generated on methanol and water oxygen atoms. Crystal data and further details concerning the crystal structure determination are found in Table 1.

Other Physical Measurements. Temperature-dependent magnetic susceptibilities were measured for $1\cdot 2H_2O\cdot 11MeOH$ by using a SQUID magnetometer (MPMS-7, Quantum Design) at 1.0 T (2.0−300K). VTVH measurements were done at 1, 4, and 7 T also in the range 2−300 K with the magnetization equidistantly sampled on a $1/T$ temperature scale. For calculations of the molar magnetic susceptibility, χ_M, the measured susceptibilities were corrected for the underlying diamagnetism of the sample holder and the sample by using tabulated Pascal's constants. Infrared spectra (400−4000 cm^{-1}) of solid samples were recorded either on a Bruker Vector 22 spectrometer or on a Shimadzu FTIR 8300 as KBr disks or as nujol mulls on KBr disks. ESI and MALDI-TOF mass spectra were recorded on a Micromass Quattro LC mass spectrometer and a Bruker Reflex IV mass spectrometer, respectively.

Computational Details. The magnetic properties of $[Mn^{III}_6Fe^{III}]^{3+}$ are simulated by a full-matrix diagonalization of the Hamiltonian in eq 1.

$$\hat{H} = -2\sum_{i<j} J_{ij}\hat{\mathbf{S}}_i\cdot\hat{\mathbf{S}}_j + \sum_i D_i[\hat{\mathbf{S}}_i\cdot\mathbf{e}_i(\vartheta_i,\phi_i)]^2 + \mu_B\sum_i \mathbf{B}\cdot\bar{\bar{\mathbf{g}}}_i\cdot\hat{\mathbf{S}}_i \quad (1)$$

Here, the first sum reflects the isotropic exchange interaction between spins given by the spin vector operators $\hat{S}_i$ at sites i. A negative value of J_{ij} corresponds to an antiferromagnetic coupling. The molecular topology of $[Mn^{III}_6Fe^{III}]^{3+}$ requires a coupling scheme consisting of two exchange interactions: one between the manganese ions in the bottom and top trinuclear building blocks, respectively, called J_{Mn-Mn} and one between the central Fe^{III} low-spin ion and all six Mn^{III} high-spin ions called J_{Fe-Mn}.

The anisotropic magnetization behavior of the manganese ions is accounted for by local anisotropy tensors in the second sum. The tensors are parametrized by a strength factor $D_i = D$, which is the same for all six manganese ions. The local unit vector $\mathbf{e}_i$, which is parametrized by polar angles ϑ_i and ϕ_i, points along the local Jahn−Teller axis and represents an easy or a hard axis depending on the sign of D. Due to the S_6 symmetry, all six local unit vectors $\mathbf{e}_i$ can be parametrized by the common polar angle between the Jahn−Teller axis and the S_6 symmetry axis, which is ϑ = 36.5°. The relative ϕ_i angles are determined by the S_6 symmetry.

The third term models the interaction with the applied magnetic field. $\mathbf{g}_i$ represents the local g tensor at site i. For the Mn^{III} ions, it assumes an isotropic value of 1.98. The first-order angular momentum in the ground state of low-spin Fe^{III} results in an anisotropic g tensor. Therefore, we have performed simulations using either an isotropic g value for low-spin Fe^{III} or an anisotropic $\mathbf{g}_{Fe^{III}}$ tensor.

The Hilbert space of the full spin-Hamiltonian has a dimension of 31 250. We employ the full S_6 symmetry. This reduces the average matrix size to roughly 5000 × 5000. Since the measurements are performed with powder samples, we also employ an orientational average using a Lebedev grid with 50 orientations.[87]

Results and Discussion

Synthesis and Characterization. Treating a solution of $[(talen^{t\text{-}Bu_2})(Mn^{III}Cl)_3]$[88] in methanol with a solution of 3.5 equiv of $K_3[Fe(CN)_6]$ in a minimal amount of water with stirring for 16 h at room temperature yields a dark suspension. Filtration resulted in an orange−yellow solid, which was identified by FTIR as unreacted $K_3[Fe(CN)_6]$, and a dark brown solution. Slow evaporation of the solvent yielded dark brown single-crystals covered with some yellow−orange powder. The single-crystals were examined by X-ray diffraction analysis (space group $P2_1/c$), resulting in the formulation $[\{(talen^{t\text{-}Bu_2})(Mn(MeOH))_3\}_2\{Fe(CN)_6\}]$-$[Fe(CN)_6]\cdot 18MeOH\cdot 2H_2O$ ($1\cdot 18MeOH\cdot 2H_2O$). FTIR spectra of **1** reveal the presence of the typical vibrations for

(84) Sheldrick, G. M. *SADABS*; University of Göttingen: Göttingen, Germany, 2001.
(85) Sheldrick, G. M. *Acta Crystallogr.* **1990**, *A46*, 467–473.
(86) Sheldrick, G. M. *Acta Crystallogr.* **2008**, *A64*, 112–122.
(87) Lebedev, V. I.; Laikov, D. N. *Dokl. Akad. Nauk* **1999**, *366*, 741.
(88) Glaser, T.; Heidemeier, M. Unpublished results.

the ligand $(talen^{t\text{-}Bu_2})^{6-}$ in the heptanuclear complexes $[M_6{}^tM^c]^{n+}$.[66] Additionally, characteristic bands for the CN vibrations of the $[Fe(CN)_6]^{3-}$ appeared in the range 2020−2140 cm^{-1} (vide infra). The ESI-MS of **1** in methanol exhibits two prominent ions at *m*/*z* 917.5 and 1376.2 with mass and isotope distribution patterns corresponding to $[\{(talen^{t\text{-}Bu_2})Mn_3\}_2\{Fe(CN)_6\}]^{3+}$ and $[\{(talen^{t\text{-}Bu_2})Mn_3\}_2\{Fe(CN)_6\}]^{2+}$, respectively. The MALDI-TOF MS exhibits only one signal at *m*/*z* 2751.0 with mass and isotope distribution pattern corresponding to $[\{(talen^{t\text{-}Bu_2})Mn_3\}_2\{Fe(CN)_6\}]^{+}$. Interestingly, the coordinated methanol molecules, which were found in the crystal structure, are not coordinated anymore in the MS, indicating the weakness of the $Mn-O^{MeOH}$ bond. The weakness of this sixth coordination site of Mn^{III} was also found in $[(talen^{NO_2})(Mn^{III}(DMSO)_2)_3](ClO_4)_3$, where the most prominent signal in the MS data corresponds to $[(talen^{NO_2})Mn_3(DMSO)_3]^{3+}$.[83] In this trinuclear Mn^{III} complex, there are two DMSO molecules coordinated to each Mn^{III} ion, with one shorter Mn−O bond (2.22 Å) and one longer bond (2.34 Å).

Visual inspection of the batches obtained by the above-mentioned procedure already indicated that these batches are not pure. In addition to some yellow−orange powder of $K_3[Fe(CN)_6]$, there are two kinds of crystals. The majority of crystals are polyhedra with some hexagonal faces and, as a minor component, some hexagonal plates. The inhomogeneity of the sample is also corroborated by elemental analysis and by the CN stretching vibrations in the FTIR spectra. There appear mainly four stretching vibrations in the 2020−2140 cm^{-1} region, varying in intensities and exact energetic position.

The precipitation of $K_3[Fe(CN)_6]$ can be attributed to the high methanol-to-water ratio in the reaction solution (note that $K_3[Fe(CN)_6]$ is insoluble in methanol). To prevent precipitation of $K_3[Fe(CN)_6]$, it was dissolved in pure methanol by the addition of 18-crown-6. We have optimized the reaction conditions by measuring the single-crystal diffraction data of each kind of crystal form obtained. In this respect, we obtained the crystal structure of **1** in a cubic crystal form and also of $[Mn^{III}_6Fe^{III}]^{3+}$ cations with other anions. In analogy to the preparation of $[Mn^{III}_6Cr^{III}]^{3+}$, the optimized synthesis to obtain pure **1** did not employ the difficult-to-synthesize precursor $[(talen^{t\text{-}Bu_2})(Mn^{III}Cl)_3]$. We synthesized the molecular building block $[(talen^{t\text{-}Bu_2})\{Mn^{III}(solv)_n\}_3]^{3+}$ in situ by reacting the ligand $H_6talen^{t\text{-}Bu_2}$ with manganese(II) acetate or manganese(II) lactate in methanol. After several optimization steps, we have found one experimental condition where we only obtained one kind of crystal. The molecular building block $[(talen^{t\text{-}Bu_2})\{Mn^{III}(solv)_n\}_3]^{3+}$ (either produced from the acetate or lactate) was reacted with a solution of $[K(18\text{-crown-}6)]_3[Fe(CN)_6]$ in methanol, which results in only one kind of crystal (polyhedra with some hexagonal faces) and some dark powder. Recrystallization from hot methanol and filtration results in the separation of only the above-mentioned kind of crystals (space group $P2_1/c$), which were analyzed as $[\{(talen^{t\text{-}Bu_2})(Mn(MeOH))_3\}_2\{Fe(CN)_6\}]\text{-}[Fe(CN)_6]\cdot 18MeOH\cdot 2H_2O$ (**1**·18MeOH·2H_2O).

IR Spectroscopy. As we envisioned problems to obtain a pure sample of only one crystal form, we have used IR spectroscopy throughout the optimization of the synthetic procedure. In analogy to one CN stretching frequency in $[Mn^{III}_6Cr^{III}]^{3+}$,[66] we expected two CN stretching frequencies for **1**: one for the ionic $[Fe(CN)_6]^{3-}$ and one at slightly higher energies for the bridging $[Fe(CN)_6]^{3-}$ of $[Mn^{III}_6Fe^{III}]^{3+}$. However, we have always observed at least 4 CN stretching frequencies. The IR spectrum of $K_3[Fe^{III}(CN)_6]$ exhibits one strong peak at 2118 cm^{-1} but some more peaks at lower energy of lower intensity. There is no consistent assignment for the origin of these additional bands in the literature. The six local CN stretching frequencies of the six cyanides in a hexacyanometallate couple to three normal modes in O_h symmetry of A_{1g} (ν_1), E_g (ν_3), and T_{1u} (ν_6) irreducible representations. The A_{1g} and the E_g modes are Raman-active, while the T_{1u} is IR-active. Several studies dealt with the assignment of the vibrations of hexacyanoferrate,[89−96] but the main focus has been on the M−C stretching frequencies at low energy.[97,98] The Raman-active vibrations of $K_3[Fe^{III}(CN)_6]$ in aqueous solution at 2131 cm^{-1} and 2124 cm^{-1} have been assigned to the A_{1g} and E_g modes, respectively.[91] The IR-active mode has been assigned to the strong band at 2105 cm^{-1} in $K_3[Fe^{III}(CN)_6]\cdot 3H_2O$,[89] 2119 cm^{-1} in $K_3[Fe^{III}(CN)_6]$,[90] and 2118 cm^{-1} in $Cs_3Li[Fe^{III}(CN)_6]$.[93] The several remaining weak bands near the strong CN stretching fundamental frequency have been assigned to combination and difference bands of CN stretching with lattice vibrations or C−M−C deformation vibrations[89] or alternatively to two isotopomers (^{13}CN and $C^{15}N$), each giving rise to a doublet.[90] Jones et al. reported the frequencies of the pure isotopomers: 2083 cm^{-1} for $Cs_3Li[Fe^{III}(^{13}CN)_6]$ and 2097 cm^{-1} for $Cs_3Li[Fe^{III}(C^{15}N)_6]$.[92] Doping of $[Fe(CN)_6]^{3-}$ in crystals of NaCl and KCl resulted in a splitting of ν_6 into three strong bands which were attributed to the symmetry reduction (D_{2h} or C_s local symmetries).[99] The effect of symmetry reduction on the ν_6 mode has also been studied for the absorption of $[Fe(CN)_6]^{3-}$ on metal electrodes.[100,101]

IR spectra of **1** measured as KBr pellets exhibits three bands of medium intensity at 2135, 2106, and 2062 cm^{-1} with an

(89) Nakagawa, I.; Shimanouchi, T. *Spectrochim. Acta* **1962**, *18*, 101–113.
(90) Dunsmuir, J. T. R.; Lane, A. P. *J. Chem. Soc. A* **1971**, 776–780.
(91) Adams, D. M.; Hooper, M. A. *Dalton Trans.* **1972**, 160–162.
(92) Jones, L. H.; Swanson, B. I.; Kubas, G. J. *J. Chem. Phys.* **1974**, *61*, 4650–4655.
(93) Swanson, B. I.; Jones, L. H. *Inorg. Chem.* **1974**, *13*, 313–316.
(94) Ohata, A.; Morioka, Y.; Nakagawa, I. *Chem. Lett.* **1981**, 239–242.
(95) Kettle, S. F. A.; Aschero, G. L.; Diana, E.; Rossetti, R.; Stanghellini, P. L. *Inorg. Chem.* **2006**, *45*, 4928–4937.
(96) Shatruck, M.; Chambers, K. E.; Prosvirin, A. V.; Dunbar, K. R. *Inorg. Chem.* **2007**, *46*, 5155–5165.
(97) Lorenzelli, V.; Delorme, P. *Spectrochim. Acta* **1963**, *19*, 2033–2045.
(98) Nakagawa, I.; Shimanouchi, T. *Spectrochim. Acta* **1970**, *26A*, 131–141.
(99) Jain, S. C.; Warrier, A. V. R.; Sehgal, H. K. *J. Phys. C: Solid State Phys.* **1973**, *6*, 193–200.
(100) Korzeniewski, C.; Severson, M. W.; Schmidt, P. P.; Pons, S.; Fleischmann, M. *J. Phys. Chem.* **1987**, *91*, 5568–5573.
(101) Kunimatsu, K.; Shigematsu, Y.; Uosaki, K.; Kita, H. *J. Electroanal. Chem.* **1989**, *262*, 195–209.

additional weak but very sharp band at 2027 cm^{-1}. We have been concerned by a report of Atanasov et al., who attributed an analogous sharp band in the IR spectra of $[Fe^{III}(CN)_6]^{3-}$-bridged chain compounds to some $[Fe^{II}(CN)_6]^{4-}$ impurities. The origin of these impurities was assigned to a slow reduction of iron(III) under synthetic conditions.[102] However, Mössbauer spectroscopy on several batches of **1** provides no indication for the presence of an Fe^{II} species (vide infra).

In order to probe the possible reduction of $[Fe^{III}(CN)_6]^{3-}$ by Br^- of the KBr pellet, we have measured IR spectra of $K_3[Fe^{III}(CN)_6]$ as KBr pellets with different times used for grinding of the sample with KBr. Interestingly, the main CN vibration shifts to slightly higher energy from 2118 to 2122 cm^{-1}. However, even more surprisingly, the low-intensity bands change with an increase in the grinding time. The intensity of the 2075 cm^{-1} bands decreases, and a new sharp band at 2027 cm^{-1} appears. We attribute these changes to increasing amounts of reduction of $[Fe^{III}(CN)_6]^{3-}$ by Br^- to $[Fe^{II}(CN)_6]^{4-}$. In order to prevent this possible reduction, we measured IR spectra of $K_3[Fe^{III}(CN)_6]$ and **1** in nujol. The IR spectrum of $K_3[Fe^{III}(CN)_6]$ simplifies to the main vibration at 2116 cm^{-1} and one low-intensity peak at 2075 cm^{-1}. Thus, we assign the bands at 2045 and 2027 cm^{-1} in the IR spectra of $K_3[Fe^{III}(CN)_6]$ measured as KBr pellets to contamination with $[Fe^{II}(CN)_6]^{4-}$ obtained by reduction with Br^-.

The IR spectrum of **1** in nujol therefore exhibits only three CN stretching vibrations at 2133, 2104, and 2060 cm^{-1}. We assign the middle band to the ionic $[Fe^{III}(CN)_6]^{3-}$ and the bands at 2133 and 2060 cm^{-1} to the bridging $[Fe^{III}(CN)_6]^{3-}$ of $[Mn^{III}_6Fe^{III}]^{3+}$. The splitting might be attributed to the symmetry reduction from O_h to S_6.

Structural Characterization. **1**·$2H_2O$·18MeOH crystallizes in the space group $P2_1/c$. The asymmetric unit consists of half of the molecule. A plot of the asymmetric unit excluding noncoordinating solvent molecules with thermal ellipsoids is depicted in Figure 1. The other half of the molecule is generated by a crystallographic center of inversion, which is located at the central iron ion. The molecular structure of the trication $[\{(talen^{t\text{-}Bu_2})(Mn^{III}(MeOH))_3\}_2\{Fe^{III}(CN)_6\}]^{3+}$, $[Mn^{III}_6Fe^{III}]^{3+}$, is illustrated in various orientations and accentuations in Figure 2. The views in Figure 2a and b are perpendicular and parallel to the approximate molecular C_3 axis, respectively. The view in Figure 2b nicely illustrates the staggered conformation of the Mn^{III} salen subunits leading to a molecular S_6 axis. The approximate point group of the trication is also S_6. The electrostatic trication−trianion attraction is strong, resulting in van der Waals like contacts of the $[Fe^{III}(CN)_6]^{3-}$ counterions with the lipophilic *t*-butylphenyl equatorial ring in the trication $[Mn^{III}_6Fe^{III}]^{3+}$ (Figure 2d). This packing results in an Fe−Fe distance of the trication and the trianion of 11.46 Å and the closest intermolecular Fe−Mn distance of 6.93 Å. The closest Fe−Fe distance between two trications is 18.18 Å.

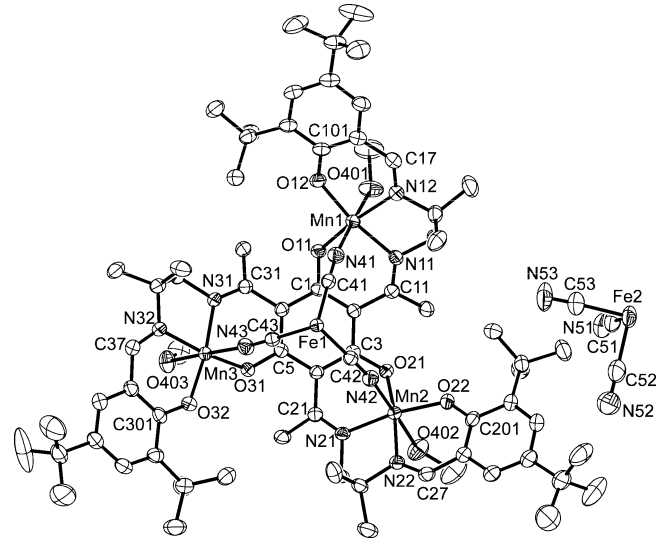

Figure 1. ORTEP plot of the asymmetric unit of crystals of **1**·18MeOH·$2H_2O$ with the numbering scheme used. Thermal ellipsoids are drawn at the 50% probability level; noncoordinating solvent molecules and hydrogen atoms are omitted for clarity.

The molecular structure of the trication $[Mn^{III}_6Fe^{III}]^{3+}$ closely resembles that of $[Mn^{III}_6Cr^{III}]^{3+}$.[66] Two trinuclear Mn^{III} triplesalen building blocks are connected by the hexacyanoferrate (Figure 2c). Each Mn^{III} is coordinated by two imine nitrogen atoms and two phenolate oxygen atoms of a salen-like ligand compartment. The coordination environment is completed by a nitrogen atom of the hexacyanoferrate and an oxygen atom of a coordinated methanol molecule. This is different from $[Mn^{III}_6Cr^{III}]^{3+}$, where the sixth position of the Mn^{III} ions is coordinated by either methanol or acetonitrile or it is empty, that is, a 5-fold coordinated Mn^{III} ion.[66] Selected bond distances and bond angles are summarized in Table 2.

The Mn^{III} ions are in an axially elongated octahedral environment. The mean values for the Mn−O bond distances for the central PhO^- and the terminal PhO^- are 1.89 and 1.88 Å, respectively, while the mean Mn−N bond distances are 1.99 and 1.98 Å for the central and the terminal imine donors, respectively. The Mn^{III} Jahn−Teller axis is along the $N^{C\equiv N}\cdots O^{MeOH}$ direction, evidenced by longer mean $Mn-N^{CN}$ and $Mn-O^{MeOH}$ bond distances of 2.19 and 2.33 Å, respectively. The spread in the individual bond distances is very small despite the $Mn-O^{MeOH}$ distances, which vary from 2.30 to 2.37 Å. This is in accordance with only weak bonding of the MeOH donors, as evidenced by their absence in the mass spectra.

An important aspect for the Mn−Fe exchange interaction is the structure of the bridging $[Fe^{III}(CN)_6]^{3-}$. The ionic $[Fe^{III}(CN)_6]^{3-}$ may be used as in internal reference, and its values are provided in parentheses. The mean Fe−C and C≡N bond distances are 1.93 Å (1.94) and 1.15 Å (1.15 Å), while the mean Fe−C≡N angle is 178.7° (178.1°). The spread of the values for the angles is 0.2° (0.5°). Thus, the coordination of the cyanide nitrogen atoms to Mn^{III} does not introduce severe strain to the bridging $[Fe^{III}(CN)_6]^{3-}$, as the Fe−C≡N units do not exhibit significant structural changes. A nonlinearity is observed in the C≡N−Mn angles, which

(102) Atanasov, M.; Comba, T.; Förster, S.; Linti, G.; Malcherek, T.; Miletich, R.; Prikhod'ko, A. I.; Wadepohl, H. *Inorg. Chem.* **2006**, *45*, 7722–7735.

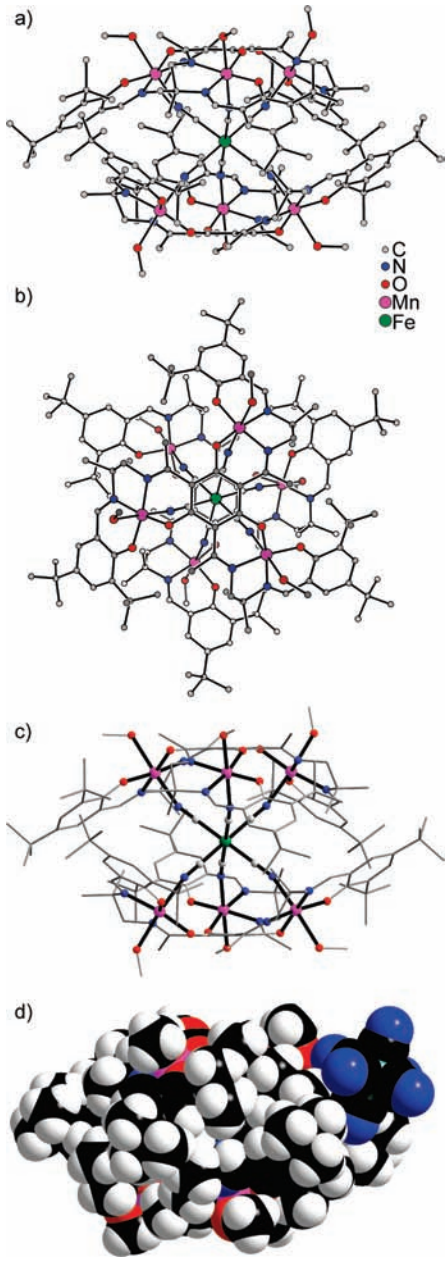

Figure 2. Molecular structure of $[\{(talen^{t\text{-}Bu_2})(Mn(MeOH))_3\}_2\{Fe(CN)_6\}]^{3+}$ in crystals of $\mathbf{1}\cdot 18MeOH\cdot 2H_2O$ drawn (a) perpendicular and (b) parallel to the approximate molecular C_3 axis. The view in b demonstrate the staggered conformation of the Mn^{III} salen subunits. The molecular structure of the trication in c resembles that shown in a but highlights the metal centers with their first-shell coordination to indicate the relative orientations of the local Mn^{III} Jahn−Teller axes. (d) Space-filling model of **1** demonstrating the close van der Waals contacts between the two trinuclear triplesalen building blocks and the van der Waals like interaction of the counteranion $[Fe(CN)_6]^{3-}$ with the heptanuclear trication.

are in the range 161.0−163.3°. This bending is common for the $(CN)_5Fe-C\equiv N-Mn$ unit. A search in the Cambridge Structural Database provided 47 individual units where the mean values (standard deviation) are 176.5° (2.0°) for the Fe−C≡N angle and 156.0° (9.8°) for the C≡N−Mn angle. Thus, the bending of the C≡N−Mn units introduces no significant strain, which would decrease the energetic driving force for the formation of the heptanuclear complexes.

The bending does not occur randomly, but all six C≡N−Mn units bent toward the molecular C_3 axis. This has an important impact on the topology of the six Mn^{III} ions surrounding the central Fe^{III} low-spin ion. In the hypothetical limit of linear C≡N−Mn angles, the six Mn^{III} ions would form an octahedral (i.e., cubic) arrangement around the central Fe^{III} low-spin ion. The concerted bending of the C≡N−Mn units leads to a symmetry reduction from ap-

Table 2. Selected Interatomic Distances [Å] and Angles [deg] for $\mathbf{1}\cdot 2H_2O\cdot 18MeOH$[a]

Mn(1)−O(11)	1.8942(18)	O(22)−Mn(2)−O(21)	97.16(8)
Mn(1)−O(12)	1.8833(19)	O(22)−Mn(2)−N(22)	91.32(9)
Mn(1)−N(11)	1.991(2)	O(21)−Mn(2)−N(22)	169.57(9)
Mn(1)−N(12)	1.988(2)	O(22)−Mn(2)−N(21)	170.46(9)
Mn(1)−N(41)	2.185(2)	O(21)−Mn(2)−N(21)	87.92(9)
Mn(1)−O(401)	2.305(2)	N(22)−Mn(2)−N(21)	82.85(9)
Mn(2)−O(21)	1.8903(18)	O(22)−Mn(2)−N(42)	94.31(9)
Mn(2)−O(22)	1.8851(19)	O(21)−Mn(2)−N(42)	90.16(9)
Mn(2)−N(21)	1.988(2)	N(22)−Mn(2)−N(42)	95.26(9)
Mn(2)−N(22)	1.982(2)	N(21)−Mn(2)−N(42)	93.75(9)
Mn(2)−N(42)	2.186(2)	O(22)−Mn(2)−O(402)	87.82(9)
Mn(2)−O(402)	2.367(2)	O(21)−Mn(2)−O(402)	88.06(8)
Mn(3)−O(31)	1.8986(19)	N(22)−Mn(2)−O(402)	86.20(9)
Mn(3)−O(32)	1.8822(19)	N(21)−Mn(2)−O(402)	84.27(9)
Mn(3)−N(31)	1.996(2)	N(42)−Mn(2)−O(402)	177.38(9)
Mn(3)−N(32)	1.981(2)	O(32)−Mn(3)−O(31)	97.02(8)
Mn(3)−N(43)	2.196(2)	O(32)−Mn(3)−N(32)	92.03(9)
Mn(3)−O(403)	2.302(2)	O(31)−Mn(3)−N(32)	168.91(9)
O(11)−C(1)	1.314(3)	O(32)−Mn(3)−N(31)	172.26(9)
O(12)−C(101)	1.326(3)	O(31)−Mn(3)−N(31)	87.67(9)
O(21)−C(3)	1.315(3)	N(32)−Mn(3)−N(31)	82.66(9)
O(22)−C(201)	1.317(3)	O(32)−Mn(3)−N(43)	93.47(9)
O(31)−C(5)	1.317(3)	O(31)−Mn(3)−N(43)	89.64(9)
O(32)−C(301)	1.319(3)	N(32)−Mn(3)−N(43)	96.22(10)
N(11)−C(11)	1.299(3)	N(31)−Mn(3)−N(43)	92.71(9)
N(12)−C(17)	1.283(4)	O(32)−Mn(3)−O(403)	87.92(9)
N(21)−C(21)	1.299(3)	O(31)−Mn(3)−O(403)	85.56(8)
N(22)−C(27)	1.289(4)	N(32)−Mn(3)−O(403)	88.39(9)
N(31)−C(31)	1.295(3)	N(31)−Mn(3)−O(403)	86.30(9)
N(32)−C(37)	1.287(4)	N(43)−Mn(3)−O(403)	175.13(9)
Mn(1)−Mn(2)	6.7403(6)	Fe(1)−Mn(1)−Mn(2)	49.704(5)
Mn(1)−Mn(3)	6.7925(6)	Fe(1)−Mn(1)−Mn(3)	49.408(5)
Mn(2)−Mn(3)	6.7786(6)	Mn(2)−Mn(1)−Mn(3)	60.117(6)
Mn(1)−Fe(1)	5.1923(4)	Fe(1)−Mn(2)−Mn(1)	49.501(5)
Mn(2)−Fe(1)	5.2080(4)	Fe(1)−Mn(2)−Mn(3)	49.483(5)
Mn(3)−Fe(1)	5.2155(4)	Mn(1)−Mn(2)−Mn(3)	60.323(6)
Fe(1)−C(41)	1.927(3)	Fe(1)−Mn(3)−Mn(2)	49.386(5)
Fe(1)−C(42)	1.931(3)	Fe(1)−Mn(3)−Mn(1)	49.111(5)
Fe(1)−C(43)	1.929(3)	Mn(2)−Mn(3)−Mn(1)	59.559(6)
N(41)−C(41)	1.153(4)	C(1)−O(11)−Mn(1)	124.08(16)
N(42)−C(42)	1.153(4)	C(101)−O(12)−Mn(1)	130.99(18)
N(43)−C(43)	1.144(4)	C(3)−O(21)−Mn(2)	123.29(16)
Fe(2)−C(51)	1.940(4)	C(201)−O(22)−Mn(2)	131.50(18)
Fe(2)−C(52)	1.938(4)	C(5)−O(31)−Mn(3)	123.48(16)
Fe(2)−C(53)	1.939(4)	C(301)−O(32)−Mn(3)	131.07(18)
C(51)−N(51)	1.148(5)	C(41)−Fe(1)−C(43)	91.28(11)
C(52)−N(52)	1.147(5)	C(41)−Fe(1)−C(42)	90.89(11)
C(53)−N(53)	1.144(5)	C(43)−Fe(1)−C(42)	90.92(11)
O(12)−Mn(1)−O(11)	96.68(8)	Mn(1)−Fe(1)−Mn(2)	80.795(6)
O(12)−Mn(1)−N(12)	91.46(9)	Mn(1)−Fe(1)−Mn(3)	81.481(7)
O(11)−Mn(1)−N(12)	169.91(9)	Mn(2)−Fe(1)−Mn(3)	81.131(6)
O(12)−Mn(1)−N(11)	170.20(9)	C(41)−N(41)−Mn(1)	161.0(2)
O(11)−Mn(1)−N(11)	88.44(9)	C(42)−N(42)−Mn(2)	162.1(2)
N(12)−Mn(1)−N(11)	82.66(9)	C(43)−N(43)−Mn(3)	163.3(2)
O(12)−Mn(1)−N(41)	94.05(9)	N(41)−C(41)−Fe(1)	178.8(3)
O(11)−Mn(1)−N(41)	89.93(9)	N(42)−C(42)−Fe(1)	178.7(2)
N(12)−Mn(1)−N(41)	95.45(9)	N(43)−C(43)−Fe(1)	178.6(3)
N(11)−Mn(1)−N(41)	94.30(9)	C(52)−Fe(2)−C(51)	88.85(17)
O(12)−Mn(1)−O(401)	88.56(9)	C(53)−Fe(2)−C(51)	90.31(16)
O(11)−Mn(1)−O(401)	87.61(8)	C(52)−Fe(2)−C(53)	89.14(17)
N(12)−Mn(1)−O(401)	86.64(9)	N(51)−C(51)−Fe(2)	177.8(4)
N(11)−Mn(1)−O(401)	83.30(9)	N(52)−C(52)−Fe(2)	178.3(4)
N(41)−Mn(1)−O(401)	176.60(9)	N(53)−C(53)−Fe(2)	178.1(4)

[a] Symmetry transformations used to generate equivalent atoms. #1: $-x+1, -y+1, -z+1$. #2: $-x, -y+1, -z$.

proximate O_h to approximate C_3 symmetry (Figure 2c). This symmetry reduction is also evident in the Mn···Mn distances, which are shorter between the Mn^{III} ions of the same trinuclear triplesalen building block (6.77 Å) and which are longer for Mn^{III} ions belonging to different trinuclear triplesalen building blocks (7.92 Å).

An important aspect for the Mn−Mn exchange interaction is the overall geometry of the trinuclear triplesalen building block. A regular ligand folding results in an overall bowl-shaped molecular structure for the trinuclear Cu^{II} and Ni^{II} complexes of $(talen^{t\text{-}Bu_2})^{6-}$. We have applied several parameters for a quantitative description of the ligand folding in the study of the trinuclear triplesalen complexes.[15,37] It turned out that the best parameters to quantitatively describe the ligand folding are the bent angles $\varphi_{central}$ and $\varphi_{terminal}$. The bent angle φ (introduced by Cavallo and Jacobsen)[103] is defined by $\varphi = 180° - \angle(M{-}X_{NO}{-}X_R)$ (X_{NO}, midpoint of adjacent N and O donor atoms; X_R, midpoint of the six-membered chelate ring containing the N and O donor atoms). This bent angle is best suited to differentiate between a bending along an idealized line through neighboring N and O ligands and a line perpendicular to the former, resulting in a helical distortion (see Scheme 3 in ref 15).[15] In the trinuclear Ni^{II} and Cu^{II} complexes, $\varphi_{central}$ is in the range 20−30°, while $\varphi_{terminal}$ is significantly smaller in the range 3−9°. Coordination of a hexacyanometallate should obviously increases the ligand folding. The mean bent angle at the terminal phenolates in $[Mn^{III}_6Fe^{III}]^{3+}$ is still small at $\varphi_{terminal} = 7.9°$ (spread 3.9°), while the mean bent angle at the central phenolates increases to $\varphi_{central} = 36.0°$ (spread 2.7°).

It is interesting to compare these values to those in $[Mn^{III}_6Cr^{III}]^{3+}$: $\varphi_{terminal} = 8.5°$ (spread 3.6°) and $\varphi_{central} = 46.7°$ (spread 9.2°).[66] Surprisingly, the bending in $[Mn^{III}_6Cr^{III}]^{3+}$ is stronger (by ∼10°) in comparison to $[Mn^{III}_6Fe^{III}]^{3+}$, although the Fe−C bond distance of 1.93 Å is significantly shorter in comparison to the Cr−C bond distance of 2.07 Å. In a simple assumption, the shorter Fe−C bond should result in an overall smaller hexacyanometallate unit and therefore force the trinuclear Mn^{III} triplesalen unit to a more pronounced bending to obtain an optimized orientation for bonding to the three nitrogen donors. A close inspection of the foldings in $[Mn^{III}_6Fe^{III}]^{3+}$ and $[Mn^{III}_6Cr^{III}]^{3+}$ indicates a stronger helical distortion in $[Mn^{III}_6Fe^{III}]^{3+}$ (Figure 3). In $[Mn^{III}_6Fe^{III}]^{3+}$, the six carbon atoms and the three oxygen atoms of the phloroglucinol lie in one plane with the ketimine carbon atoms (Figure 3a left). On the other hand, the phloroglucinol unit in $[Mn^{III}_6Cr^{III}]^{3+}$ is slightly distorted, with the oxygen atoms lying below this plane toward the hexacyanochromate and the ketimine carbon atoms above this plane (Figure 3b left).

This distortion corresponds to a helical distortion, which may be best visualized by the angle between the benzene plane and the vector formed by the central phenolate oxygen atom and the central ketimine nitrogen atom. This is indicated in Figure 3, on the right. The calculated angles are 11.7°

(103) Cavallo, L.; Jacobsen, H. *Eur. J. Inorg. Chem.* **2003**, 892–902.

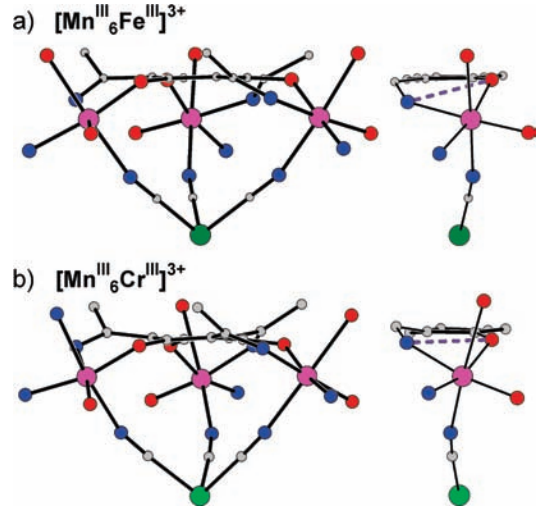

Figure 3. Sections of the molecular structures of (a) $[Mn^{III}_6Fe^{III}]^{3+}$ and (b) $[Mn^{III}_6Cr^{III}]^{3+}$,[66] with the view direction in the benzene plane of the central phloroglucinol to illustrate the difference in the folding of the trinuclear Mn^{III} triplesalen building blocks. Note that the view directions for the left and right panels are slightly different, but the view directions on the left panel are the same and the view directions on the right panel are the same. The dashed purple lines in the right panels represent the vector defined by $O^{Ph}{-}N^{ketimine}$ to visualize the angle between this vector and the central benzene plane.

(spread 1.2°) for $[Mn^{III}_6Fe^{III}]^{3+}$ and 1.3° (spread 2.3°) for $[Mn^{III}_6Cr^{III}]^{3+}$, confirming the visually estimated stronger helical distortion in $[Mn^{III}_6Fe^{III}]^{3+}$.

In summary, the exchange of Cr^{III} by Fe^{III}, that is, going from $[Mn^{III}_6Cr^{III}]^{3+}$ to $[Mn^{III}_6Fe^{III}]^{3+}$, results in a smaller hexacyanometallate unit. The trinuclear Mn^{III} triplesalen building blocks have some degree of freedom to orient the three Mn^{III} ions for optimal bonding to the facially arranged cyanide nitrogen atoms. The reorientation can be formally subdivided into a bending of the O_2N_2Mn salen plane relative to the central benzene along the central $O^{Ph}{-}N^{imine}$ vector and into a helical distortion perpendicular to this vector. While the origins for the different degrees of folding versus helical distortion are not exactly known, these differences result in different orientations of the magnetic d orbitals and the phenolate p orbitals. Our studies on the trinuclear triplesalen complexes indicate that a variation of these orientations has a strong impact on the spin-polarization and spin-delocalization participations[39] and thus on the overall exchange interaction of the three Mn^{III} ions through the phloroglucinol unit.

Mössbauer Spectroscopy. Mössbauer spectra in zero magnetic field at 80 K were measured on different batches of **1**. All spectra exhibit the same broad two-line feature shown in Figure 4a. Fitting with one quadrupole doublet results in $\delta = -0.05$ mm s^{-1} and $|\Delta E_Q| = 1.17$ mm s^{-1}, but the Lorentzian lineshape does not satisfactorily reproduce the measured band shape. Due to the presence of two distinct $[Fe^{III}(CN)_6]^{3-}$ units in **1**, we fitted the data with two quadrupole doublets. The fit results in two quadrupole doublets with a nearly 1:1 ratio (not restricted). While the isomer shifts are almost identical, the quadrupole splittings differ and the doublet with smaller quadrupole splitting appears to be broader in order to reproduce the experimental

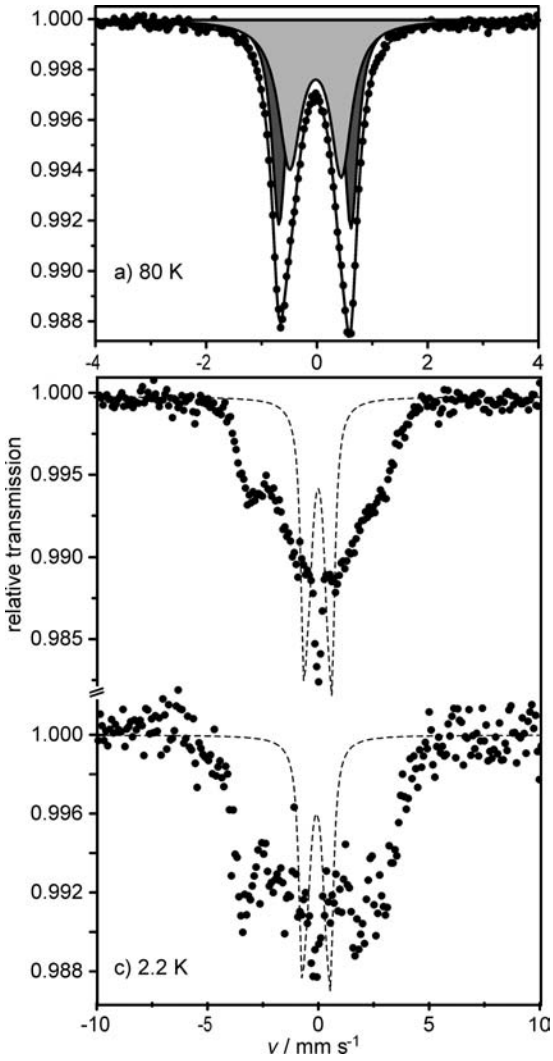

Figure 4. Temperature-dependent Mössbauer spectra measured on **1**·11MeOH·2H_2O in zero magnetic field at (a) 80, (b) 4.2, and (c) 2 K. The measured data are presented by dots. The solid line is the sum of the individual quadrupole doublets. The individual quadrupole doublets are presented by the filled Lorenzians line shapes. Dark: $\delta = -0.06$ mm s^{-1}. $|\Delta E_Q| = 1.30$ mm s^{-1}. $\Gamma = 0.31$ mm s^{-1}. Rel. area: 48% assigned to the central brigding $[Fe^{III}(CN)_6]^{3-}$ of $[Mn^{III}_6Fe^{III}]^{3+}$. Light: $\delta = -0.05$ mm s^{-1}. $|\Delta E_Q| = 0.96$ mm s^{-1}. $\Gamma = 0.46$ mm s^{-1}. Rel. area: 52% assigned to the ionic $[Fe^{III}(CN)_6]^{3-}$. Note the wider velocity range for the *x* axis in b and c. The dashed line in b and c is the sum of the simulated quadruple doublets of the 80 K spectrum in a scaled in intensity as a guide to the eyes for the positions of the quadruple doublets, if no magnetic splitting would occur.

band shape (Figure 4a). The final data are $\delta = -0.06$ mm s^{-1} and $|\Delta E_Q| = 1.30$ mm s^{-1} for the dark doublet in Figure 2a and $\delta = -0.05$ mm s^{-1} and $|\Delta E_Q| = 0.93$ mm s^{-1} for the light doublet in Figure 4a.

We have measured the starting material $K_3[Fe^{III}(CN)_6]$, which yields $\delta = -0.05$ mm s^{-1} and $|\Delta E_Q| = 0.49$ mm s^{-1}. Therefore, we assign the quadrupole doublet with the smaller quadrupole splitting to the ionic $[Fe^{III}(CN)_6]^{3-}$. Since the classical paper of Oosterhuis and Lang on $K_3[Fe^{III}(CN)_6]$,[104] Mössbauer spectroscopy has been applied extensively on hexacyanoferrates. The quadrupole splitting of $[Fe^{III}(CN)_6]^{3-}$ strongly depends on the exact surroundings, that is, the crystal structure. The low crystal symmetry in **1** already perturbs the ionic $[Fe^{III}(CN)_6]^{3-}$, but the symmetry reduction from approximate O_h to S_6 introduces a stronger perturbation and results in a larger quadrupole splitting for the bridging $[Fe^{III}(CN)_6]^{3-}$.

The Mössbauer spectra measured at 4.2 K (Figure 4b) and 2.0 K (Figure 4c) in zero external magnetic field reveal magnetically split spectra. Interestingly, both $[Fe^{III}(CN)_6]^{3-}$ subspectra seem to split magnetically, as no unperturbed quadrupole doublet is evident in the region found in the 80 K spectra (Figure 4). Samples of $K_3[Fe^{III}(CN)_6]$ do not split magnetically in zero external magnetic fields.[104] However, diluted samples in $K_3[Co^{III}(CN)_6]$ as a diamagnetic host lattice split magnetically without applied magnetic fields at low temperatures due to the absence of effective spin−spin and spin−lattice relaxation pathways. Thus, it is interesting to note that the close proximity of Mn^{III} ions to the Fe^{III} low-spin ion in **1** leads to magnetic splittings, although effective spin−spin relaxation paths are present. Therefore, we attribute this behavior to a slow relaxation of the magnetization in **1** on the Mössbauer timescale.

Magnetic Measurements. Temperature-dependent magnetic susceptibility measurements (2−290 K, 1 T) on powdered samples of **1**·2H_2O·11MeOH reveal $\mu_{eff} = 12.15\mu_B$ at 290 K, which decreases monotonically with decreasing temperature to a minimum of $5.82\mu_B$ at 2 K (Figure 5). The room-temperature value is close to the spin-only value ($g_i = 2.0$) of six uncoupled Mn^{III} high-spin ions ($S_i = 2$) and two uncoupled Fe^{III} low-spin ions ($S_i = 1/2$) of 12.25 μ_B. Using more reasonable *g* values[105] for Mn^{III} of 1.98 and for Fe^{III} low-spin ions of 2.1 matches the experimental value even better at 12.16 μ_B.

The continuous decrease of μ_{eff} indicates dominating antiferromagnetic interactions between the metal ions. However, antiferromagnetic interactions between the central Fe^{III} low-spin ion and the Mn^{III} ions should result in an increase of μ_{eff} at lower temperatures due to a ferrimagnetic coupling scheme, as observed in $[Mn^{III}_6Cr^{III}]^{3+}$.[66] Therefore, the continuous decrease of μ_{eff} with decreasing temperatures might indicate that the magnetic anisotropy has a stronger effect than the exchange interaction.

We have performed VTVH magnetization measurements for **1** at 1, 4, and 7 T (Figure 6). The isofield lines exhibit a strong nesting behavior, which is indicative of strong magnetic anisotropy.[106] This is corroborated by the small value for the saturation magnetization even at the highest field of 7 T of 14.2 μ_B.

In order to obtain some quantitative insight into magnitudes and ratios of the exchange couplings J_{ij} and zero-field splittings D_i, we have performed a full-matrix diagonalization of the appropriate spin-Hamiltonian, including isotropic HDvV exchange, zero-field splitting, and Zeeman interaction (see the Experimental Section). A frequently used simplifica-

(104) Oosterhuis, W. T.; Lang, G. *Phys. Rev.* **1969**, *178*, 439–456.

(105) Figgis, B. N. *Introduction to Ligand Fields*; Interscience Publishers: New York, 1964.

(106) Girerd, J.-J.; Journaux, Y. In *Physical Methods in Bioinorganic Chemistry*; Que, L. J., Ed.; University Science Books: Sausalito, CA, 2000; pp 321−374.

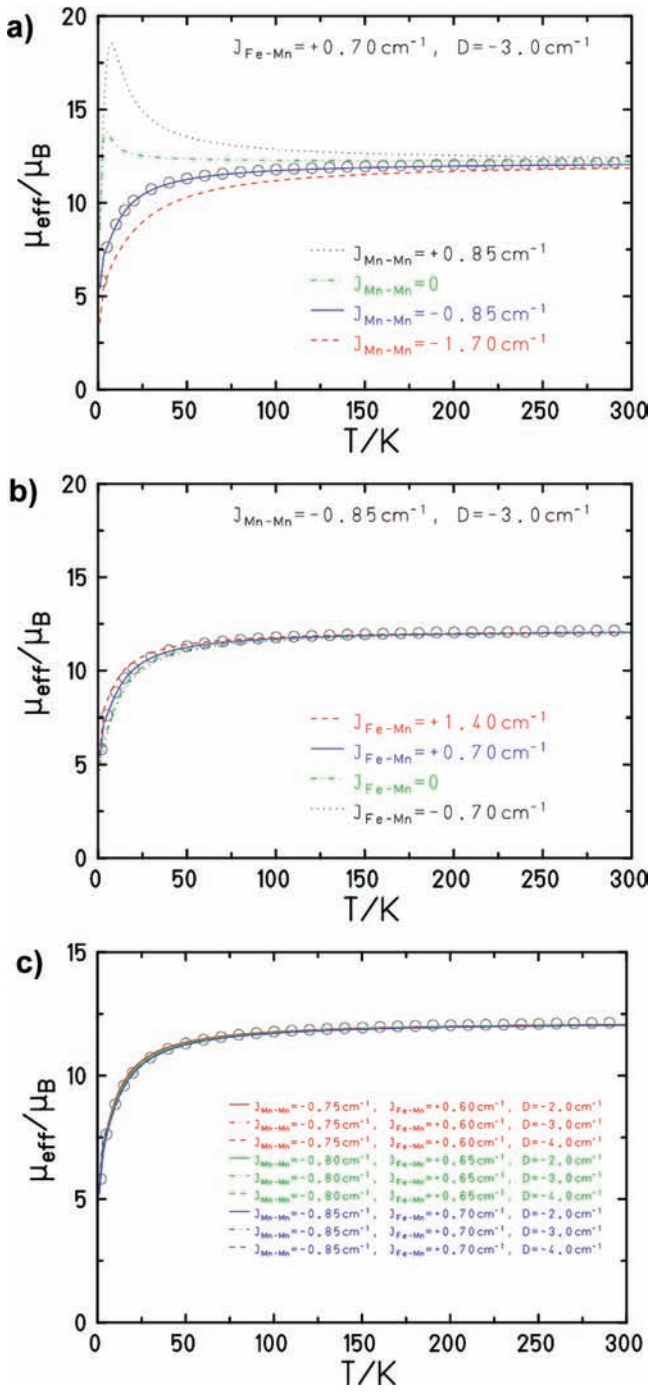

Figure 5. Temperature dependence of μ_{eff} at 1 T for **1**·2H$_2$O·11MeOH. Experimental data given as circles. The lines correspond to simulations based on the complete spin-Hamiltonian by full-matrix diagonalitzation. The simulations are performed with fixed parameters despite variation of J_{Mn-Mn} in a; of J_{Fe-Mn} in b; and of D_{Mn}, J_{Mn-Mn}, and J_{Fe-Mn} in c.

tion in such spin-Hamiltonians is a collinearity of the local **D** tensors, which is not always the case. We have incorporated the zero-field splitting for the Mn^{III} ions including the relative orientations of the individual **D** tensors by the angle ϑ of the Jahn−Teller axis with the molecular axis. The topology of $[Mn^{III}_6Fe^{III}]^{3+}$ requires a coupling scheme with two different coupling constants: J_{Fe-Mn} describes the interaction between the central Fe^{III} low-spin ion ($\mathbf{S_7}$) with each Mn^{III} ($\mathbf{S_1}$ to $\mathbf{S_6}$), and J_{Mn-Mn} describes the interaction between two Mn^{III}'s in a trinuclear triplesalen subunit. The HDvV part of the full spin-Hamiltonian (see eq 1) is specified for this molecule in eq 2.

$$H_{HDvV} = -2J_{Fe-Mn}(\mathbf{S_1S_7}+\mathbf{S_2S_7}+\mathbf{S_3S_7}+\mathbf{S_4S_7}+\mathbf{S_5S_7}+\mathbf{S_6S_7}) - 2J_{Mn-Mn}(\mathbf{S_1S_2}+\mathbf{S_2S_3}+\mathbf{S_3S_1}+\mathbf{S_4S_5}+\mathbf{S_5S_6}+\mathbf{S_6S_4}) \quad (2)$$

The counterion $[Fe^{III}(CN)_6]^{3-}$ was treated as an additional uncoupled spin of $S_i = 1/2$ with $g_i = 2.1$. For the central Fe^{III} low-spin ion in the trigonal elongated octahedral environment, $\mathbf{g}_{Fe}$ is modeled by one value along the C_3 axis, that is, $g_{Fe}^{\parallel} = 2.0$, and by another one in the perpendicular directions, that is, $g_{Fe}^{\perp} = 2.4$.[102,105,107,108] However, no significant differences have been observed in the simulations by using an isotropic $g_{Fe} = 2.1$ also for the central Fe^{III} low-spin ion of $[Mn^{III}_6Fe^{III}]^{3+}$. This insensitivity can be attributed to the small contribution of the $S_{Fe} = 1/2$ to the overall magnetic moment.

We have performed several simulations varying J_{Mn-Mn}, J_{Fe-Mn}, and D_{Mn} in order to obtain a qualitative understanding of the influence of the individual parameters on the bulk magnetization curves. In Figure 5, we have summarized some simulations with two parameters fixed close to the final values and variation of the third parameter for the μ_{eff} versus T data.

Figure 5a shows variations of J_{Mn-Mn} with fixed $J_{Fe-Mn} = +0.70$ cm^{-1} and $D_{Mn} = -3.0$ cm^{-1}. It is quite evident that the experimental decrease of μ_{eff} with a decrease of T requires a slightly antiferromagnetic J_{Mn-Mn}. For the chosen parameters of J_{Mn-Mn} and D_{Mn}, $J_{Fe-Mn} = -0.85$ cm^{-1} seems quite reasonable.

Figure 5b shows the variation of J_{Fe-Mn} with fixed $J_{Mn-Mn} = -0.85$ cm^{-1} and $D_{Mn} = -3.0$ cm^{-1}. The sign and magnitude of J_{Fe-Mn} have only a minor influence on the temperature dependence of μ_{eff}, since this interaction couples only the small Fe^{III} spin ($S_{Fe} = 1/2$) to the much larger Mn^{III} spin ($S_{Mn} = 2$). The effect of D_{Mn} by various combinations of J_{Mn-Mn} and J_{Fe-Mn} is shown in Figure 5c. As it is well established,[106] zero-field splitting effects have only minor influence on μ_{eff} versus T curves. In order to evaluate the influence of D_{Mn}, field-dependent measurements at low temperatures are necessary. These data are provided in Figure 6.

It is important to note that the zero-field splitting terms, the HDvV terms, and the Zeeman terms of the full spin-Hamiltonian, eq. 1, are all on the same order of magnitude. This leads to a complex field- and orientation-dependent mixing of m_S wave functions, so that S_t is not a good quantum number to describe the system. The simple approximation by using only one ground spin state, S_t, cannot adequately describe this field- and orientation-dependent mixing of m_S wave functions. However, the use of the full spin-Hamiltonian for the VTVH data therefore not only provides a good measure for D_{Mn} but also allows the determination of J_{Mn-Mn} and J_{Mn-Fe}.

(107) Taylor, C. P. S. *Biochim. Biophys. Acta* **1977**, *491*, 137–149.
(108) Atanasov, M.; Comba, T.; Daul, C. A. *Inorg. Chem.* **2008**, *47*, 2449–2463.

Figure 6a provides the variation of J_{Mn-Mn} with fixed $J_{Fe-Mn} = +0.70$ cm^{-1} and $D_{Mn} = -3$ cm^{-1}. These simulations corroborate the interpretation of those in Figure 5a, that J_{Mn-Mn} is slightly antiferromagnetic. $J_{Mn-Mn} = -0.85$ cm^{-1} fits well for the fixed values of J_{Fe-Mn} and D_{Mn}. The influence of J_{Fe-Mn} is less pronounced, as seen in Figure 6b ($J_{Mn-Mn} = -0.85$ cm^{-1} and $D_{Mn} = -3.0$ cm^{-1}), but provides preference for a slight ferromagnetic coupling of $J_{Fe-Mn} = 0.70$ cm^{-1}.

The influence of D is shown in Figure 6c for various combinations for J_{Mn-Mn} and J_{Fe-Mn}. Interestingly changes in the second digit in J_{Mn-Mn} and J_{Fe-Mn} influence the simulated curves at the same magnitude as do changes of 1 cm^{-1} in D_{Mn}. Simulations with different angles ϑ were performed, but only angles around the experimentally found value of 36.5° provide satisfactory reproductions of the magnetic data.

We do not intend to obtain a perfect simulation of the experimental data with one unique set of parameters, as there are more effects like non-negligible orbital effects on the exchange coupling in low-spin iron(III), the occurrence of intermolecular couplings, and the lower molecular symmetry in the solid state, which are beyond the employed Hamiltonian. However, the simulations of the VTVH data in Figure 6 provide better reproductions for the 4 and 7 T data and more deviations for the 1 T data. We assume that intermolecular dipolar interactions between the large magnetic moments of $[Mn^{III}_6Fe^{III}]^{3+}$ are quite active at 1 T, despite the large intermolecular distances, while the higher fields of 4 and 7 T break down these dipolar interactions more efficiently. This leads to a better validity of the pure molecular approximation for the simulations. On the other hand, these effects indicate the presence of quite strong intermolecular interactions. Nevertheless, for the conclusions drawn in this article, this would not yield any new insight. A reasonable range of parameters that reproduces both the temperature-dependent magnetization at 1 T and the VTVH magnetization data at 1, 4, and 7 T is $J_{Mn-Mn} = -(0.85 \pm 0.15)$ cm^{-1}, $J_{Fe-Mn} = +(0.70 \pm 0.30)$ cm^{-1}, and $D_{Mn} = -(3.0 \pm 0.7)$ cm^{-1}.

Discussion on the Exchange Coupling Constants. The exchange coupling of the unit $(NC)_5Fe-C\equiv N-Mn^{III}$(salen), where salen stands for a general salen-like ligand, has been investigated several times.[67−69,71,78,79,109−112] According to the first and second Goodenough−Kanomori rules,[26,113−116] this Fe^{III} low-spin (t_{2g}^5)—Mn^{III} high-spin ($t_{2g}^3e_g^1$) system would exhibit both antiferromagnetic (t_{2g}—t_{2g}) and ferromagnetic pathways (t_{2g}—e_g), respectively. As usual, the antiferromagnetic pathways are stronger in comparison to ferromagnetic pathways. Additional pathways of lower strength arise according to the third Goodenough−Kanamori rule, like the ferromagnetic pathway Fe^{III} (e_g^0)—Mn^{III} (e_g^1). However, such an analysis is only valid in the hypothetical limit of regular O_h symmetry for both ions with the C≡N$^-$ linker along the z axis and no rotation of the two local xy axes. Real $(NC)_5Fe-C\equiv N-Mn^{III}$(salen) systems exhibit several degrees of distortion in comparison to the ideal symmetry: bending of the C≡N−Mn angle, rotation of the

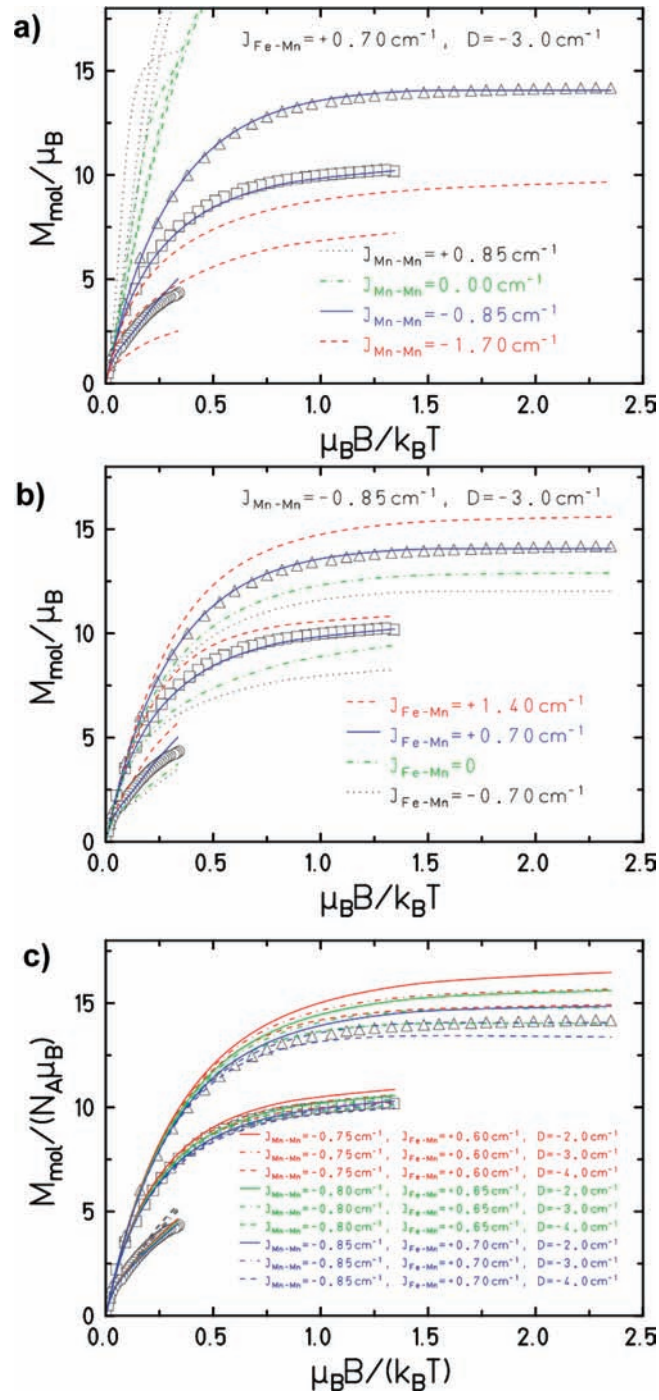

Figure 6. VTVH magnetization measurements at 1 T (circles), 4 T (squares), and 7 T (triangles). The lines correspond to simulations based on the complete spin-Hamiltonian by full-matrix diagonalitzation. The simulations are performed with fixed parameters despite variation of J_{Mn-Mn} in a; of J_{Fe-Mn} in b; and of D_{Mn}, J_{Mn-Mn}, and J_{Fe-Mn} in c.

(109) Miyasaka, H.; Takahashi, H.; Madanbahsi, T.; Sugiura, K.-I.; Clerac, R.; Nojiri, H. *Inorg. Chem.* **2005**, *44*, 5969–5971.
(110) Ni, Z.-H.; Kou, H.-Z.; Zhang, L.-F.; Ge, C.; Cui, A.-L.; Wang, R.-J.; Li, Y.; Sato, O. *Angew. Chem., Int. Ed.* **2005**, *44*, 7742–7745.
(111) Wen, H.-R.; Wang, C.-F.; Li, Y.-Z.; Zuo, J. L.; Song, Y.; You, X.-Z. *Inorg. Chem.* **2006**, *45*, 7032–7034.
(112) Ni, W.-W.; Ni, Z.-H.; Cui, A.-L.; Liang, X.; Kou, H.-Z. *Inorg. Chem.* **2007**, *46*, 22–33.
(113) Goodenough, J. B. *Magnetism and the Chemical Bond*; Interscience: New York, 1963.
(114) Anderson, P. W. *Phys. Rev.* **1959**, *115*, 2–13.
(115) Anderson, P. W. *Magnetism*; Academic Press: New York, 1963.
(116) Weihe, H.; Güdel, H. U. *Inorg. Chem.* **1997**, *36*, 3632–3639.

local *xy*-coordinate systems relative to each other, bending of the equatorial coordination planes with respect to C≡N vector, and many more. Emperically, C≡N−Mn angles close to 150° have been proposed to favor ferromagnetic couplings, while angles >161° favor antiferromagnetic interactions.[109] However, the C≡N−Mn angles in **1** are in the range 161−163°, and also in other systems, antiferromagnetic interactions have been observed for angles of 155°.[110] The rotations of the *xy* planes relative to each other account for a weakening of the antiferromagnetic t_{2g}−t_{2g} pathway, which should be zero for a relative rotation of 45°.[112] To the best of our knowledge, there are no commonly accepted magneto-structural correlations for the $(NC)_5Fe-C\equiv N-Mn^{III}$(salen) unit taking both of these obvious geometrical distortions. However, the occurrence of ferro- as well as antiferromagnetic interactions depending on the actual coordination geometries is well accepted.

The coupling constant $J_{Mn-Mn} = -(0.85 \pm 0.15)$ cm^{-1} observed in **1** is close to the value of $J_{Mn-Mn} = -1.03$ cm^{-1} obtained for $[Mn^{III}_6Cr^{III}]^{3+}$ [66] and in the range of $J_{Mn-Mn} = -(0.30 \pm 0.05)$ cm^{-1} for $[(talen^{NO_2})\{Mn^{III}(DMSO)_2\}_3](ClO_4)_3$.[83] These results seem to indicate that the exchange coupling through the phloroglucinol bridging unit is antiferromagnetic in nature for Mn^{III} ions despite the ferromagnetic couplings observed in trinuclear Cu^{II} complexes[35−37] and a V^{IV}=O complex.[38] We have analyzed the ferromagnetic couplings in these complexes with respect to the molecular structures and found that the crucial parameter for an efficient spin-polarization mechanism through the bridging benzene unit seems to be the amount of spin density in the p_z^{π} orbitals of the phenolic oxygen atoms.[39] This spin density crucially depends on the metal ion, the remaining coordination sites, and the ligand folding at the central metal−phenolate bond. The spin transfer from the metal to the phenolate oxygen atom occurs by two different mechanisms, namely, spin-polarization and spin-delocalization, which can provide opposing contributions. We are currently investigating more heptanuclear complexes $[Mn^{III}_6M^c]^{n+}$ to obtain experimental insight into the dependence of the exchange coupling of Mn^{III} ions through the phloroglucinol bridging unit from structural parameters, especially the ligand folding.

Conclusions

We have synthesized and characterized structurally as well as magnetically the heptanuclear complex $[Mn^{III}_6Fe^{III}]^{3+}$ in the form of its hexacyanoferrate salt. The synthesis follows the same rationale as the synthesis of the corresponding heptanuclear complex $[Mn^{III}_6Cr^{III}]^{3+}$,[66] which has an $S_t = 21/2$ spin ground state with significant magnetic anisotropy and exhibitis single-molecule magnet behavior. The molecular structure of $[Mn^{III}_6Fe^{III}]^{3+}$ matches the molecular structure of the $[Mn^{III}_6Cr^{III}]^{3+}$. Thus, we have successfully prepared the second example of this general series $[M^t_6M^c]^{n+}$. This illustrates the driving force for the building of these heptanuclear complexes by molecular recognition of three molecular building blocks, that is, two trinuclear manganese triplesalen units and one hexacyanometallate, in analogy to the key−lock principle.

The trinuclear triplesalen building blocks exhibit a ligand folding of the individual manganese salen subunits, which gives rise to an overall bowl-shaped structure. This ligand folding preorganizes the three Mn^{III} ions for coordination to the three facially arranged nitrogen atoms of a hexacyanometallate. The different sizes of the hexacyanoferrate in comparison to hexacyanochromate in combination with a close inspection of the details of the molecular structures establishes that the manganese triplesalen building blocks exhibit some degree of freedom in their ligand folding to orient the manganese ion for an optimized binding overlap with the hexacyanometallate group. This degree of freedom in the ligand folding can be formally subdivided into a ligand folding along the phenolate oxygen-ketimine nitrogen vector and a helical distortion perpendicular to this vector. A comparison of the molecular structures exhibits a stronger helical distortion in $[Mn^{III}_6Fe^{III}]^{3+}$ than in $[Mn^{III}_6Cr^{III}]^{3+}$. This different ligand folding has an influence on the relative orientations of the phenolate oxygen p orbitals to the manganese d orbitals, which should result in differences in the Mn^{III} Mn^{III} exchange interactions.

The heptanuclear complexes are not only stable in the solid state but also in solution, as has been evidenced by ESI-MS. While the molecular structures in the solid state exhibit a methanol molecule coordinated to each Mn^{III} ion in $[Mn^{III}_6Fe^{III}]^{3+}$, the MS data (ESI and MALDI-TOF) only exhibit peaks for 5-fold coordinated Mn^{III} ions; that is, the coordinated methanol molecules have been dissociated. This is indicative of a weak Mn^{III}−methanol bond in the sixth coordination site. This is corroborated by the strongest spread of all bond distances for the $Mn-O^{MeOH}$ bond distances. In $[Mn^{III}_6Cr^{III}]^{3+}$, the sixth position of the Mn^{III} ion has been filled by either methanol molecules or acetonitrile molecules, or the sixth position was empty; that is, the Mn^{III} ion is only 5-fold coordinated.

This illustrates the inherent feature of Mn^{III}−salen units that a coordination number of five is sufficient to satisfy the electronic needs of Mn^{III}. The strong electron-donating properties of the salen ligand in combination with the Jahn−Teller effect may be accounted for by this property. Thus, the coordination of this sixth position at each Mn^{III} is difficult to control in the synthetic procedure. *The weakness of this solvent−Mn^{III} bond indicates a limit in the rational design of single-molecule magnets.* Differences in the coordination environments of the six Mn^{III} ions result in a reduction of the overall molecular symmetry from C_3 symmetry. This introduces some rhombicity and therefore a higher probability for the quantum tunnelling of the magnetization through the anisotropy barrier.

The temperature-dependence of μ_{eff} for **1** exhibits a steady decrease with decreasing temperature. In order to understand the contributions of the individual exchange coupling interaction, the zero-field splitting, and the saturation effects by the Zeeman interaction, we have performed a full-matrix diagonalization of the spin-Hamiltonian, taking into account

all these interactions. Although the Hilbert space of the matrix is 62 500 (for $[Mn^{III}_6Fe^{III}]^{3+}$and the counteranion $[Fe^{III}(CN)_6]^{3-}$), efficient theoretical methods developed by one of us[117−119] make problems of this size manageable. This approach provides more accurate insight into the electronic structure, as does the utilization of one spin state to describe the low-temperature data (so-called *giant-spin approach*). Very recently, a detailed analysis of the magnetic data utilizing the full spin-Hamiltonian has been reported for the high-T_B SMM Mn_6.[120]

The combined simulation of the temperature dependence of μ_{eff} and the VTVH data has provided a meaningful set of parameters, $J_{Mn-Mn} = -(0.85 \pm 0.15)$ cm^{-1}, $J_{Fe-Mn} = +(0.70 \pm 0.30)$ cm^{-1}, and $D_{Mn} = -(3.0 \pm 0.7)$ cm^{-1}, which demonstrates only weak coupling between the paramagnetic centers but sizable zero-field splitting of the salen Mn^{III} unit. Due to the occurrence of weak antiferromagnetic interactions of the Mn^{III} ions through the phloroglucinol bridging unit, the coupling of the Mn^{III} ions with the central metal ion of the hexacyanometallate must be stronger in order to obtain a stronger stabilization of the spin ground state. The coupling of the Mn^{III} ions with the Cr^{III} ions of the bridging hexacyanochromate in $[Mn^{III}_6Cr^{III}]^{3+}$ [66] was found to be $J_{Cr-Mn} = -5.0$ cm^{-1}. This results in the stabilization of a high-spin ground state of $S_t = 21/2$ and points to a SMM. The small coupling $J_{Fe-Mn} = +(0.70 \pm 0.30)$ cm^{-1} in $[Mn^{III}_6Fe^{III}]^{3+}$ results in a strong mixing of m_S wave functions of various spin states, so that no high spin ground state is stabilized. Thus, the reason for $[Mn^{III}_6Cr^{III}]^{3+}$ being a SMM and for $[Mn^{III}_6Fe^{III}]^{3+}$ not being a SMM is the small J_{Fe-Mn} coupling. We are currently synthesizing and characterizing more examples of the general series $[M^t_6M^c]^{n+}$ to obtain better SMMs.

Acknowledgment. This work was supported by the Fonds der Chemischen Industrie, the BMBF, the Dr. Otto Röhm Gedächtnisstiftung, and the DFG (SFB 424).

Supporting Information Available: Additional information in CIF format. This material is available free of charge via the Internet at http://pubs.acs.org.

IC8016529

(117) Schnack, J.; Brüger, M.; Luban, M.; Kögerler, P.; Morosan, E.; Fuchs, R.; Modler, R.; Nojiri, H.; Rai, R. C.; Cao, J.; Musfeldt, J. L.; Wei, X. *Phys. Rev. B: Condens. Matter Mater. Phys.* **2006**, *73*, 094401.
(118) Postnikov, A.; M.; Brüger, M.; Schnack, J. *Phase Transitions* **2005**, *78*, 47–59.
(119) Schnack, J. In *Lecture Notes in Physics 645*; Springer: Berlin, 2004; pp 155−194.
(120) Carretta, S.; Guidi, T.; Santini, P.; Amoretti, G.; Pieper, O.; Lake, B.; Slageren, J. v.; El Hallak, F.; Wernsdorder, W.; Mutka, H.; Russina, M.; Milios, C. J.; Brechin, E. K. *Phys. Rev. Lett.* **2008**, *100*, 157203.